Personalized Federated Learning through Local Memorization

Othmane Marfoq, Laetitia Kameni, Richard Vidal, Giovanni Neglia

Personalized Federated Learning through Local Memorization

Othmane Marfoq [1 2] **Giovanni Neglia** [1] **Laetitia Kameni** [2] **Richard Vidal** [2]

Abstract

Federated learning allows clients to collaboratively learn statistical models while keeping their data local. Federated learning was originally used to train a unique global model to be served to all clients, but this approach might be sub-optimal when clients' local data distributions are heterogeneous. In order to tackle this limitation, recent *personalized federated learning* methods train a separate model for each client while still leveraging the knowledge available at other clients. In this work, we exploit the ability of deep neural networks to extract high quality vectorial representations (embeddings) from non-tabular data, e.g., images and text, to propose a personalization mechanism based on local memorization. Personalization is obtained by interpolating a collectively trained global model with a local k-nearest neighbors (kNN) model based on the shared representation provided by the global model. We provide generalization bounds for the proposed approach in the case of binary classification, and we show on a suite of federated datasets that this approach achieves significantly higher accuracy and fairness than state-of-the-art methods.

1. Introduction

Heterogeneity is a core and fundamental challenge in Federated Learning (FL) (Li et al., 2020; Kairouz et al., 2019). Indeed, clients highly differ both in size and distribution of their local datasets (*statistical heterogeneity*), and in their storage and computational capabilities (*system heterogeneity*). Those two aspects challenge the assumption that clients should train a common global model, as pursued in many federated learning papers (McMahan et al., 2017; Konečny et al., 2016; Sahu et al., 2018; Karimireddy et al., 2020; Mohri et al., 2019). In fact, all clients should be content with a model's architecture constrained by the minimum common capabilities. Even when clients have similar hardware (e.g., they are all smartphones), in presence of statistical heterogeneity, a global model may be arbitrarily bad for some clients raising important fairness concerns (Li et al., 2021).

Motivated by the recent success of memorization techniques based on nearest neighbours for natural language processing, (Khandelwal et al., 2019; 2020), computer vision (Papernot and McDaniel, 2018; Orhan, 2018), and few-shot classification (Snell et al., 2017; Wang et al., 2019), we propose `kNN-Per`, a personalized FL algorithm based on local memorization. `kNN-Per` combines a global model trained collectively (e.g., via `FedAvg` (McMahan et al., 2017)) with a kNN model on a client's local datastore. The global model also provides the shared representation used by the local kNN. Local memorization at each FL client can capture the client's local distribution shift with respect to the global distribution. Indeed, our experiments show that memorization is more beneficial when the distribution shift is larger. The generalization bound in Sec. 3 contributes to justify our empirical findings as well as those in (Khandelwal et al., 2019; 2020; Orhan, 2018).

`kNN-Per` offers a simple and effective way to address statistical heterogeneity even in a dynamic environment where client's data distributions change after training. It is indeed sufficient to update the local datastore with new data without the need to retrain the global model. Moreover, each client can independently tune the local kNN to its storage and computing capabilities, partially relieving the most powerful clients from the need to align their model to the weakest ones. Finally, `kNN-Per` has a limited leakage of private information, as personalization only occurs once communication exchanges have ended, and, if needed, it can be easily combined with differential privacy techniques.

Our contributions are threefold: 1) we propose `kNN-Per`, a simple personalization mechanism based on local memorization; 2) we provide generalization bounds for the proposed approach in the case of binary classification; 3) through extensive experiments on FL benchmarks, we show that `kNN-Per` achieves significantly higher accuracy and fairness than state-of-the-art methods.

The paper is organized as follows. After an overview of

[1]Inria, Université Côte d'Azur, Sophia Antipolis, France [2]Accenture Labs, Sophia Antipolis, France. Correspondence to: Othmane Marfoq <othmane.marfoq@inria.fr>.

Proceedings of the 39^{th} International Conference on Machine Learning, Baltimore, Maryland, USA, PMLR 162, 2022.

related work in Sec. 2, we present kNN-Per in Sec. 3 and provide generalization bounds in Sec. 4. Experimental setup and results are described in Sec. 5 and Sec. 6, respectively.

2. Related Work

We discuss personalized FL approaches to address statistical heterogeneity and system heterogeneity as well as nearest neighbours augmented neural networks.

2.1. Statistical Heterogeneity

This body of work considers that all clients have the same model architecture but potentially different parameters.

A simple approach for FL personalization is learning first a global model and then fine-tuning its parameters at each client through stochastic gradient descent for a few epochs (Jiang et al., 2019; Yu et al., 2020); we refer later to this approach as FedAvg+. FedAvg+ was later studied by Chen and Chao (2022) and Cheng et al. (2021). The global model can then be considered as a meta-model to be used as initialization for a few-shot adaptation at each client. Later work (Khodak et al., 2019; Fallah et al., 2020; Acar et al., 2021) has formally established the connection with Model Agnostic Meta Learning (MAML) (Jiang et al., 2019) and proposed different algorithms to train a more suitable meta-model for local personalization.

ClusteredFL (Sattler et al., 2020; Ghosh et al., 2020; Mansour et al., 2020) assumes that clients can be partitioned into several clusters, with clients in the same cluster sharing the same model, while models can be arbitrarily different across clusters. Clients jointly learn during training the cluster to which they belong as well as the cluster model. FedEM (Marfoq et al., 2021) can be considered as a soft clustering algorithm as clients learn personalized models as mixtures of a limited number of component models.

Multi-Task Learning (MTL) allows for more nuanced relations among clients' models by defining federated MTL as a penalized optimization problem, where the penalization term captures clients' dissimilarity. Seminal work (Smith et al., 2017; Vanhaesebrouck et al., 2017; Zantedeschi et al., 2020) proposed algorithms able to deal with quite generic penalization terms, at the cost of learning only linear models or linear combinations of pre-trained models. Other MTL-based algorithms (Hanzely and Richtárik, 2020; Hanzely et al., 2020; T. Dinh et al., 2020; Dinh et al., 2021; Li et al., 2021; Huang et al., 2021; Li et al., 2021) are able to train more general models but consider simpler penalization terms (e.g., the distance to the average model).

An alternative approach is to interpolate a global model and one local model per client (Deng et al., 2020; Corinzia and Buhmann, 2019; Mansour et al., 2020). Zhang et al. (2021) extended this idea by letting each client interpolate the local models of other clients with opportune weights learned during training. Our algorithm, kNN-Per, also interpolates a global and a local model, but the global model plays a double role as it is also used to provide a useful representation for the local kNN.

Closer to our approach, FedRep (Collins et al., 2021), FedPer (Arivazhagan et al., 2019), and pFedGP (Achituve et al., 2021) jointly learn a global latent representation and local models—linear models for FedRep and FedPer, Gaussian processes for pFedGP—that operate on top of this representation. In these algorithms, the progressive refinement of local models affects the shared representation. On the contrary, in kNN-Per only the global model (and then the shared representation) is the object of federated training, and the shared representation is not influenced by local models, which are learned separately by each client in a second moment. Our experiments suggest that kNN-Per's approach is more efficient. A possible explanation is that jointly learning the shared representation and the local models lead to potentially conflicting and interfering goals. A similar argument was provided by Li et al. (2021) to justify why Ditto replaces, as penalization term, the distance from the average of the local models—as proposed in (Hanzely and Richtárik, 2020; Hanzely et al., 2020; T. Dinh et al., 2020)—with the distance from an independently learned global model. Liang et al. (2020) proposed a someway opposite approach to FedRep, FedPer, and pFedGP by using local representations as input to a global model, but the representations and the global model are still jointly learned. An additional advantage of kNN-Per's clear separation between global and local model training is that, because each client does not share any information about its local model with the server, the risk of leaking private information is reduced. In particular, kNN-Per enjoys the same privacy guarantees as FedAvg, and can be easily combined with differential privacy techniques (Wei et al., 2020).

To the best of our knowledge, pFedGP and kNN-Per are the first attempts to learn semi-parametric models (Bickel et al., 1998) in a federated setting. pFedGP relies on Gaussian processes and then has higher computational cost than kNN-Per both at training and inference.

2.2. System Heterogeneity

Some FL application scenarios envision clients with highly heterogeneous hardware, like smartphones, IoT devices, edge computing servers, and the cloud. Ideally, each client could learn a potentially different model architecture, suited to its capabilities. Such system heterogeneity has been studied much less than statistical heterogeneity.

Some work (Lin et al., 2020; Li and Wang, 2019; Zhu et al.,

2021; Zhang and Yuan, 2021) proposed to address system heterogeneity by distilling the knowledge from a global teacher to clients' student models with different architectures. While early methods (Li and Wang, 2019; Lin et al., 2020) required the access to an extra (unlabeled) public dataset, more recent ones (Zhu et al., 2021; Zhang and Yuan, 2021) eliminated this requirement.

Some papers (Diao et al., 2020; Horváth et al., 2021; Pilet et al., 2021) propose that each client only trains a sub-model of a global model. The sub-model size is determined by the client's computational capabilities. The approach appears particularly advantageous for convolutional neural networks with clients selecting only a limited subset of channels.

Tan et al. (2022) followed another approach where devices and server communicate prototypes, i.e., average representations for all samples in a given class, instead of communicating model's gradients or parameters, allowing each client to have a different model architecture and input space.

While in this paper we assume that `kNN-Per` relies on a shared global model, it is possible to replace it with heterogeneous models adapted to the clients' capabilities and jointly trained following one of the methods listed above. Then, `kNN-Per`'s interpolation with a kNN model extends these methods to address not only system heterogeneity, but also statistical heterogeneity.

To the best of our knowledge, the only existing method that takes into account both system and statistical heterogeneity is `pFedHN` (Shamsian et al., 2021). `pFedHN` feeds local clients representations to a global (across clients) hypernetwork, which can output personalized heterogeneous models. Unfortunately, the hypernetwork has a large memory footprint already for small clients' models (e.g., the hypernetwork in the experiments in (Shamsian et al., 2021) has 100 more parameters than the output model): it is not clear if `pFedHN` can scale to complex models.

We observe that `kNN-Per`'s kNN model can itself be adapted to client's capabilities by tuning the size of the datastore and/or selecting an appropriate approximate kNN algorithm, like FAISS (Johnson et al., 2019), HNSW (Malkov and Yashunin, 2020), or ProtoNN (Gupta et al., 2017) for IoT resource-scarce devices, e.g., based on Arduino.

2.3. Nearest Neighbours Augmented Neural Networks

Recent work proposed to augment neural networks with nearest neighbours classifiers for applications to language modelling (Khandelwal et al., 2019), neural machine translation (Khandelwal et al., 2020), computer vision (Papernot and McDaniel, 2018; Orhan, 2018), and few-shot learning (Snell et al., 2017; Wang et al., 2019).

In (Khandelwal et al., 2019; 2020) kNN improves model performance by memorizing explicitly (rather than implicitly in model parameters) rare patterns. Papernot and McDaniel (2018) and Orhan (2018) showed that memorization can also increase the robustness of models against adversarial attacks. Differently from these lines of work, our paper shows that local memorization at each FL client can capture the client's local distribution shift with respect to the global distribution. In this sense, our use of kNN is more similar to what is proposed for few shot learning in (Snell et al., 2017; Wang et al., 2019), where an embedding function is learned for future application to new small datasets. Beside the different learning problem, the algorithms proposed in (Snell et al., 2017; Wang et al., 2019) do not rely on models' interpolation and do not enjoy generalization guarantees as `kNN-Per` does. Moreover, their natural extension to the FL setting would lead to jointly learn the shared representation and the local kNN models, a potentially less efficient approach than ours as we discussed above when presenting `FedRep`, and `pFedGP`.

3. `kNN-Per` Algorithm

In this work we consider M classification or regression tasks also called clients. Each client $m \in [M]$ has a local dataset $\mathcal{S}_m = \left\{ s_m^{(i)} = \left(\mathbf{x}_m^{(i)}, \, y_m^{(i)} \right), 1 \leq i \leq n_m \right\}$ with n_m samples drawn i.i.d. from a distribution $\mathcal{D}_m$ over the domain $\mathcal{X} \times \mathcal{Y}$. Local data distributions $\{\mathcal{D}_m\}_{m \in [M]}$ are in general different, thus it is natural to fit a separate model (hypothesis) $h_m \in \mathcal{H}$ to each data distribution $\mathcal{D}_m$. We consider that each hypothesis $h \in \mathcal{H}$ is a discriminative model mapping each input $\mathbf{x} \in \mathcal{X}$ to a probability distribution over the set $\mathcal{Y}$, i.e., $h : \mathcal{X} \mapsto \Delta^{|\mathcal{Y}|}$, where Δ^C denotes the unitary simplex of dimension C. A hypothesis then can be interpreted as (an estimation of) a conditional probability distribution $\mathcal{D}(y|\mathbf{x})$.

Personalized FL aims to solve (in parallel) the following optimization problems

$$\forall m \in [M], \quad h_m^* \in \arg\min_{h \in \mathcal{H}} \mathcal{L}_{\mathcal{D}_m}(h), \tag{1}$$

where $[M]$ denotes the set of positive integers up to M, $l : \Delta^{|\mathcal{Y}|} \times \mathcal{Y} \mapsto \mathbb{R}^+$ is the loss function,[1] and $\mathcal{L}_{\mathcal{D}_m}(h_m) = \mathbb{E}_{(\mathbf{x},y)\sim\mathcal{D}_m}\left[l(h_m(\mathbf{x}), y)\right]$ is the true risk of a model h_m under data distribution $\mathcal{D}_m$.

We suppose that all tasks have access to a global discriminative model $h_{\mathcal{S}}$ minimizing the empirical risk on the aggregated dataset $\mathcal{S} \triangleq \bigcup_{m=1}^{M} \mathcal{S}_m$, i.e.,

$$h_{\mathcal{S}} \in \arg\min_{h \in \mathcal{H}} \mathcal{L}_{\mathcal{S}}(h), \tag{2}$$

where $\mathcal{L}_{\mathcal{S}}(h) \triangleq \sum_{m=1}^{M} \frac{n_m}{n} \cdot \frac{1}{n_m} \sum_{i=1}^{n_m} l\left(h\left(\mathbf{x}_m^{(i)}\right), y_m^{(i)}\right)$,

[1] In the case of (multi-output) regression, we have $h_m : \mathcal{X} \mapsto \mathbb{R}^d$ for some $d \geq 1$ and $l : \mathbb{R}^d \times \mathbb{R}^d \mapsto \mathbb{R}^+$.

and $n = \sum_{m=1}^{M} n_m$. Typically $h_{\mathcal{S}}$ is a feed-forward neural network, jointly trained by the clients using a standard FL algorithm like `FedAvg`.

We also suppose that the global model can be used to compute a fixed-length representation for any input $\mathbf{x} \in \mathcal{X}$, and we use $\phi_{h_{\mathcal{S}}} : \mathcal{X} \mapsto \mathbb{R}^p$ to denote the function that maps the input $\mathbf{x} \in \mathcal{X}$ to its representation. The intermediate representation can be, for example, the output of the last convolutional layer in the case of CNNs, or the last hidden state in the case of recurrent networks or the output of an arbitrary self-attention layer in the case of transformers. Note that an alternative possible approach would be to separately learn an independent shared representation, e.g., using metric learning techniques (Bellet et al., 2015).

Our method (see Algorithm 1) involves augmenting the global model with a local nearest neighbors' retrieval mechanism at each client. The proposed method does not need any additional training; it only requires a single forward pass over the local dataset S_m, $m \in [M]$: client m computes the intermediate representation $\phi_{h_{\mathcal{S}}}(\mathbf{x})$ for each sample $(\mathbf{x}, y) \in \mathcal{S}_m$. The corresponding representation-label pairs are stored in a local key-value datastore $(\mathcal{K}_m, \mathcal{V}_m)$ that is queried during inference. Formally,

$$(\mathcal{K}_m, \mathcal{V}_m) = \left\{ \left(\phi_{h_{\mathcal{S}}} \left(\mathbf{x}_m^{(i)} \right), y_m^{(i)} \right), \forall \left(\mathbf{x}_m^{(i)}, y_m^{(i)} \right) \in \mathcal{S}_m \right\}. \tag{3}$$

At inference time, given input data $\mathbf{x} \in \mathcal{X}$, client $m \in [M]$ computes $h_{\mathcal{S}}(\mathbf{x})$ and the intermediate representation $\phi_{h_{\mathcal{S}}}(\mathbf{x})$. Then, it queries its local datastore $(\mathcal{K}_m, \mathcal{V}_m)$ with $\phi_{h_{\mathcal{S}}}(\mathbf{x})$ to retrieve its k-nearest neighbors $\mathcal{N}_m^{(k)}(\mathbf{x})$ according to a distance $d(\cdot, \cdot)$:

$$\mathcal{N}_m^{(k)}(\mathbf{x}) = \left(\phi_{h_{\mathcal{S}}} \left(\mathbf{x}_{\pi_m^{(i)}(\mathbf{x})} \right), y_{\pi_m^{(i)}(\mathbf{x})} \right)_{1 \le i \le k}, \tag{4}$$

where $\pi_m^{(1)}(\mathbf{x}), \ldots, \pi_m^{(n_m)}(\mathbf{x})$ is a permutation of $[n_m]$ corresponding to the distance of the samples in $\mathcal{S}_m$ from $\mathbf{x}$, i.e., for $i \in [n_m - 1]$,

$$d\Big(\phi_{h_{\mathcal{S}}}(\mathbf{x}), \phi_{h_{\mathcal{S}}}\left(\mathbf{x}_{\pi_m^{(i)}(\mathbf{x})}\right)\Big) \le d\Big(\phi_{h_{\mathcal{S}}}(\mathbf{x}), \phi_{h_{\mathcal{S}}}\left(\mathbf{x}_{\pi_m^{(i+1)}(\mathbf{x})}\right)\Big). \tag{5}$$

Then, the client computes a local hypothesis $h_{\mathcal{S}_m}^{(k)}$ which estimates the conditional probability $\mathcal{D}_m(y|\mathbf{x})$ using a kNN method, e.g., with a Gaussian kernel:

$$\left[h_{\mathcal{S}_m}^{(k)}(\mathbf{x}) \right]_y \propto \sum_{i=1}^{k} \mathbb{1}_{\left\{ y = y_{\pi_m^{(i)}(\mathbf{x})} \right\}} \times \exp\left\{ -d\left(\phi_{h_{\mathcal{S}}}(\mathbf{x}), \phi_{h_{\mathcal{S}}}\left(\mathbf{x}_{\pi_m^{(i)}(\mathbf{x})} \right) \right) \right\}. \tag{6}$$

Algorithm 1 `kNN-Per` (Typical usage)

Learn global model using available clients with `FedAvg`.
for each client $m \in [M]$ (in parallel) **do**
  Build datastore using $\mathcal{S}_m$.
  At inference on $\mathbf{x} \in \mathcal{X}$, return $h_{m,\lambda_m}(\mathbf{x})$ given by (7)
end for

The final decision rule (hypothesis) at client $m \in [M]$ (h_{m,λ_m}) is obtained interpolating the nearest neighbour distribution $h_{\mathcal{S}_m}^{(k)}$ with the distribution obtained from the global model $h_{\mathcal{S}}$ using a hyper-parameter $\lambda_m \in (0, 1)$ to produce the final prediction, i.e.,

$$h_{m,\lambda_m}(\mathbf{x}) \triangleq \lambda_m \cdot h_{\mathcal{S}_m}^{(k)}(\mathbf{x}) + (1 - \lambda_m) \cdot h_{\mathcal{S}}(\mathbf{x}). \tag{7}$$

As h_{m,λ_m} may not belong to $\mathcal{H}$, we are considering an *improper learning* setting. The parameter λ_m is tuned at client m through a local validation dataset or cross-validation as in (Corinzia and Buhmann, 2019; Mansour et al., 2020; Zhang et al., 2021; Li et al., 2021). Clients could also use different values k_m and different distance metrics $d_m(\cdot)$, but, in what follows, we consider them equal across clients. Also our experiments in Sec. 6 show that k and $d(\cdot)$ do not require careful tuning.

4. Generalization Bounds

In this section we provide a generalization bound associated with the proposed approach in the case of binary classification, namely $\mathcal{Y} = \{0, 1\}$, when only one neighbour is used for kNN estimation, i.e., $k = 1$, and $d(\cdot, \cdot)$ is the Euclidean distance. For client $m \in [M]$, we denote by $\eta_m : \mathcal{X} \mapsto \mathbb{R}$ the true conditional probability of label 1, that is

$$\eta_m(\mathbf{x}) = \mathcal{D}_m(y = 1|\mathbf{x}). \tag{8}$$

Our result holds under the following assumptions:

Assumption 1 (Bounded representation)**.** $\phi_{h_{\mathcal{S}}} : \mathcal{X} \mapsto [0, 1]^p$.

Assumption 2 (Bounded loss)**.** $l : \Delta^{|\mathcal{Y}|} \times \mathcal{Y} \mapsto [0, 1]$. *Moreover, for* $y, y' \in \{0, 1\}$, $l(\mathbf{e}_y, y') = \mathbb{1}_{y \neq y'}$, *where* $\mathbf{e}_y \in \Delta^{|\mathcal{Y}|}$ *is the vector having all entries equal to* 0 *except the entry on the* y*-th coordinate.*

Remark 1. *Loss boundedness is a common assumption, e.g., (Mansour et al., 2020),(Shalev-Shwartz and Ben-David, 2014, Ch. 4). The second requirement is that the maximum loss is achieved when the model is fully confident about a prediction, but this is wrong. A simple transformation of common loss functions—e.g., exponentiating the logistic function—make them satisfy Assumption 2.*

Assumption 3 (Loss convexity)**.** *The loss function is convex*

on the first variable

$$\forall y_1, y_2 \in \Delta^{|\mathcal{Y}|}, \forall y \in \mathcal{Y},\ \forall \lambda_m \in [0,1], \\ l(\lambda_m \cdot y_1 + (1-\lambda_m)\cdot y_2, y) \leq \\ \lambda_m \cdot l(y_1, y) + (1-\lambda_m)\cdot l(y_2, y). \tag{9}$$

Remark 2. *Assumption 3 holds for most loss functions used in supervised machine learning, including the* mean squared error *loss, the* cross-entropy *loss, and the* hinge loss.

Assumption 4. *There exist constants $\gamma_1, \gamma_2 > 0$, such that for any dataset $\mathcal{S}$ drawn from $\mathcal{X} \times \mathcal{Y}$ and any data points $\mathbf{x}, \mathbf{x}' \in \mathcal{X}$, we have*

$$\left|\eta_m(\mathbf{x}) - \eta_m(\mathbf{x}')\right| \leq d\left(\phi_{h_\mathcal{S}}(\mathbf{x}), \phi_{h_\mathcal{S}}(\mathbf{x}')\right) \times \\ \left(\gamma_1 + \gamma_2\left(\mathcal{L}_{\mathcal{D}_m}(h_\mathcal{S}) - \mathcal{L}_{\mathcal{D}_m}(h_m^*)\right)\right), \tag{10}$$

where $h_m^* \in \arg\min_{h\in\mathcal{H}} \mathcal{L}_{D_m}(h)$.

This assumption means that if two samples $\mathbf{x}$ and $\mathbf{x}'$ have close representations $\phi_{h_\mathcal{S}}(\mathbf{x})$ and $\phi_{h_\mathcal{S}}(\mathbf{x}')$, then their labels are likely to be the same ($|\eta_m(\mathbf{x}) - \eta_m(\mathbf{x}')|$ is small). This is all the more so, the better $h_\mathcal{S}$ predictions are for distribution $\mathcal{D}_m$, $m \in [M]$ (the smaller $\mathcal{L}_{\mathcal{D}_m}(h_\mathcal{S}) - \mathcal{L}_{\mathcal{D}_m}(h_m^*)$ is). Experimental results support Assumption 4 (see Figure 3).

Our generalization bound depends, as usual, on the complexity of the hypothesis class $\mathcal{H}$ (expressed by its VC-dimension, $d_\mathcal{H}$) and on the size of the local and global datasets (n_m and n, respectively), but also on the distance between the local distribution $\mathcal{D}_m$ and the average distribution $\bar{\mathcal{D}} = \sum_{m=1}^M \frac{n_m}{n}\cdot\mathcal{D}_m$, which is the one the global model $h_\mathcal{S}$ is targeting (see (2)). The distance between two distributions $\mathcal{D}$ and $\mathcal{D}'$ associated to a hypothesis class $\mathcal{H}$ can be quantified by the *label discrepancy* (Mansour et al., 2020):

$$\mathrm{disc}_\mathcal{H}(\mathcal{D}, \mathcal{D}') = \max_{h\in\mathcal{H}} \left|\mathcal{L}_\mathcal{D}(h) - \mathcal{L}_{\mathcal{D}'}(h)\right|. \tag{11}$$

Theorem 4.1. *Suppose that Assumptions 1–4 hold, and consider $m \in [M]$ and $\lambda_m \in (0,1)$, then there exist constants c_1, c_2, c_3, c_4, and $c_5 \in \mathbb{R}$, such that*

$$\begin{aligned}
&\mathop{\mathbb{E}}_{\mathcal{S}\sim\otimes_{m=1}^M \mathcal{D}_m^{n_m}} \left[\mathcal{L}_{\mathcal{D}_m}(h_{m,\lambda_m})\right] \leq (1+\lambda_m)\cdot\mathcal{L}_{\mathcal{D}_m}(h_m^*) \\
&+ c_1(1-\lambda_m)\cdot\mathrm{disc}_\mathcal{H}\left(\bar{\mathcal{D}}, \mathcal{D}_m\right) \\
&+ c_2\lambda_m \cdot \frac{\sqrt{p}}{\sqrt[p+1]{n_m}} \cdot \left(\mathrm{disc}_\mathcal{H}\left(\bar{\mathcal{D}}, \mathcal{D}_m\right) + 1\right) \\
&+ c_3(1-\lambda_m)\cdot\sqrt{\frac{d_\mathcal{H}}{n}}\cdot\sqrt{c_4 + \log\left(\frac{n}{d_\mathcal{H}}\right)} \\
&+ c_5\lambda_m\cdot\sqrt{\frac{d_\mathcal{H}}{n}}\cdot\sqrt{c_4+\log\left(\frac{n}{d_\mathcal{H}}\right)}\cdot\frac{\sqrt{p}}{\sqrt[p+1]{n_m}},
\end{aligned} \tag{12}$$

where $d_\mathcal{H}$ is the the VC dimension of the hypothesis class $\mathcal{H}$, $n = \sum_{m=1}^M n_m$, $\bar{\mathcal{D}} = \sum_{m=1}^M \frac{n_m}{n}\cdot\mathcal{D}_m$, p is the dimension of representations, and $\mathrm{disc}_\mathcal{H}$ is the label discrepancy associated to the hypothesis class $\mathcal{H}$.

The proof of Theorem 4.1 is in Appendix A. Let us consider, for simplicity, the non-agnostic case, i.e, $\mathcal{L}_{\mathcal{D}_m}(h_m^*) = 0$. We observe that, when clients only use the global model ($\lambda_m = 0$), our generalization bound is analogous to the probabilistic bound in (Mansour et al., 2020, Eq. (2)). In particular, if data is i.i.d. distributed across the clients ($\mathrm{disc}_\mathcal{H}\left(\bar{\mathcal{D}}, \mathcal{D}_m\right) = 0$), the difference between the expected losses of the learned model and the optimal one decreases with rate $\tilde{\mathcal{O}}\left(\sqrt{\frac{d_\mathcal{H}}{n}}\right)$. Instead, when each client only uses the kNN model ($\lambda_m = 1$),[2] we recover the kNN generalization bound in (Shalev-Shwartz and Ben-David, 2014, Thm 19.3).

The bound (12) leads to predict that client m should give a larger weight ($\lambda_m > 1/2$) to its kNN model, when n_m exceeds a given threshold, even when local distributions are identical. The bound contributes then to explain why adding a memorization mechanism on top of a pretrained model can improve performance, as observed in (Khandelwal et al., 2019) and (Khandelwal et al., 2020). While it is difficult to quantify the threshold analytically (also because the constants involved depend on γ_1 and γ_2 in Assumption 4), our experiments in Sec. 6 show that even clients with a few tens of samples weigh more the kNN model than the global one.

5. Experimental Setup

We evaluate `kNN-Per` on four federated datasets spanning a wide range of machine learning tasks: language modeling (Shakespeare (Caldas et al., 2018; McMahan et al., 2017)), image classification (CIFAR-10 and CIFAR-100 (Krizhevsky, 2009)), handwritten character recognition (FEMNIST (Caldas et al., 2018)). Unless otherwise said, `kNN-Per`'s global model $h_\mathcal{S}$ is trained by all clients through `FedAvg`. Code is available at `https://github.com/omarfoq/knn-per`.

Datasets. For Shakespeare and FEMNIST datasets there is a natural way to partition data through clients (by character and by writer, respectively). We relied on common approaches in the literature to sample heterogenous local datasets from CIFAR-10 and CIFAR-100. We created a federated version of CIFAR-10 by randomly partitioning the dataset among clients using a symmetric Dirichlet distribution, as done in (Wang et al., 2020). In particular, for each label y we sampled a vector p_y from a Dirichlet distribution of order $M = 200$ and parameter $\alpha = 0.3$ (unless otherwise

[2] Note that the kNN model still relies on the representation provided by the global model.

Table 1. Datasets and models.

DATASET	TASK	CLIENTS	TOTAL SAMPLES	MODEL
FEMNIST	HANDWRITTEN CHARACTER RECOGNITION	3,550	805,263	MOBILENET-V2
CIFAR-10	IMAGE CLASSIFICATION	200	60,000	MOBILENET-V2
CIFAR-100	IMAGE CLASSIFICATION	200	60,000	MOBILENET-V2
SHAKESPEARE	NEXT-CHARACTER PREDICTION	778	4,226,158	STACKED-LSTM

specified) and allocated to client m a $p_{y,m}$ fraction of all training instances of class y. The approach ensures that the number of data points and label distributions are unbalanced across clients. For CIFAR-100, we exploit the availability of "coarse" and "fine" label structure, to partition the dataset using pachinko allocation method (Li and McCallum, 2006) as in (Reddi et al., 2021). The method generates local datasets with heterogeneous distributions by combining a per-client Dirichlet distribution with parameter $\alpha = 0.3$ (unless otherwise specified) over the coarse labels and a per-coarse-label Dirichlet distribution with parameter $\beta = 10$ over the corresponding fine labels. We also partitioned CIFAR-10 and CIFAR-100 in a different way following (Achituve et al., 2021): each client has only samples from two and ten classes for CIFAR-10 and CIFAR-100, respectively. We refer to the resulting datasets as CIFAR-10 (v2) and CIFAR-100 (v2). For FEMNIST and Shakespeare, we randomly split each local dataset into training (60%), validation (20%), and test (20%) sets. For CIFAR-10 and CIFAR-100, we maintained the original training/test data split and used 20% of the training dataset as validation dataset. Table 1 summarizes datasets, models and number of clients.

Models and representations. For CIFAR-100, CIFAR-10, and FEMNIST, we used MobileNet-v2 (Sandler et al., 2018) as a base model with the output of the last hidden layer—a 1280-dimensional vector—as representation. For Shakespeare, the base model was a stacked LSTM model with two layers, each of them with 256 units; a 1024-dimensional representation was obtained by concatenating the hidden states and the cell states.

Benchmarks. We compared `kNN-Per` with locally trained models (with no collaboration across clients) and `FedAvg` (McMahan et al., 2017), as well as with one method for each of the personalization approaches described in Sec. 2, namely, `FedAvg+` (Jiang et al., 2019),[3] `ClusteredFL` (Sattler et al., 2020), `Ditto` (Li et al., 2021), `FedRep` (Collins et al., 2021), `APFL` (Deng et al., 2020), and `pFedGP` (Achituve et al., 2021).[4] For each method, and each dataset, we tuned the learning rate via grid search on the values $\{10^{-0.5}, 10^{-1}, 10^{-1.5}, 10^{-2}, 10^{-2.5}\}$. `FedPer`'s learning rate for network heads' training was separately tuned on the same grid. `Ditto`'s penalization parameter λ_m was selected among the values $\{10^{1}, 10^{0}, 10^{-1}, 10^{-2}\}$ on a per-client basis. For `ClusteredFL`, we used the same values of tolerance specified in its official implementation (Sattler et al., 2020). We found tuning `tol1` and `tol2` particularly hard: no empirical rule is provided in (Sattler et al., 2020), and the few random settings we tried did not show any improvement in comparison to the default ones. For `APFL`, the mixing parameter α was tuned via grid search on the grid $\{0.1, 0.3, 0.5, 0.7, 0.9\}$. For `pFedGP`, we used the same hyperparameters as in (Achituve et al., 2021). The parameter λ_m of `kNN-Per` was tuned for each client via grid search on the grid $\{0.0, 0.1, 0.3, 0.5, 0.7, 0.9, 1.0\}$, and the number of neighbours was set to $k = 10$. Once the optimal hyperparameters' values were selected, models were retrained on the concatenation of training and validation sets.

Training details. In all experiments with CIFAR-10 and CIFAR-100, training spanned 200 rounds with full clients' participation at each round for all methods. The learning rate was reduced by a factor 10 at round 100 and then again at round 150. For Shakespeare, 10% of clients were sampled uniformly at random without replacement at each round, and we trained for 300 rounds with a constant learning rate. For FEMNIST, 5% of the clients participated at each round for a total 1000 rounds, with the learning rate dropping by a factor 10 at round 500 and 750. In all our experiments we employed the following aggregation scheme

$$\mathbf{w}_{t+1} = \sum_{m \notin \mathbb{S}_t} \frac{n_m}{n} \mathbf{w}_t + \sum_{m \in \mathbb{S}_t} \frac{n_m}{n} \mathbf{w}_t^m, \tag{13}$$

where $\mathbf{w}_t$, $\mathbf{w}_t^m$, and $\mathbb{S}_t$ denote, respectively, the global model, the updated model at client m, and the set of clients participating to training at round t.

In all our experiments, local hypotheses follow Eq. (6) with $d(\cdot)$ being the Euclidean distance. kNN retrieval relied on FAISS library (Johnson et al., 2019).

[3] We also implemented the more sophisticated first-order MAML approach from (Fallah et al., 2020), but had worse performance than `FedAvg+`.

[4] We were able to run the official `pFedGP`'s code (https://github.com/IdanAchituve/pFedGP) only on datasets partitioned as in (Achituve et al., 2021).

Table 2. Test accuracy: average across clients / bottom decile.

DATASET	LOCAL	FEDAVG	FEDAVG+	CLUSTEREDFL	DITTO	FEDREP	APFL	PFEDGP	KNN-PER (OURS)
FEMNIST	71.0 / 57.5	83.4 / 68.9	84.3 / 69.4	83.7 / 69.4	84.3 / 71.3	85.3 / 72.7	84.1 / 69.4	– / –	**88.2 / 78.8**
CIFAR-10	57.6 / 41.1	72.8 / 59.6	75.2 / 62.3	73.3 / 61.5	80.0 / 66.5	77.7 / 65.2	78.9 / 68.1	– / –	**83.0 / 71.4**
CIFAR-10 (V2)	82.4 / 71.3	67.9 / 60.1	85.0 / 79.6	79.9 / 72.3	86.3 / 80.6	89.1 / 85.3	82.6 / 76.4	88.9 / 84.1	**93.8 / 88.2**
CIFAR-100	31.5 / 19.8	47.4 / 36.0	51.4 / 41.1	47.2 / 36.2	52.0 / 41.4	53.2 / 41.7	51.7 / 41.1	– / –	**55.0 / 43.6**
CIFAR-100 (V2)	45.7 / 38.2	42.3 / 34.8	48.1 / 41.9	43.5 / 37.2	48.7 / 40.3	70.1 / 65.2	48.3 / 42.1	61.1 / 50.0	**74.6 / 67.3**
SHAKESPEARE	32.0 / 16.0	48.1 / 43.1	47.0 / 42.2	46.7 / 41.4	47.9 / 42.6	47.2 / 42.3	45.9 / 42.4	– / –	**51.4 / 45.4**

Table 3. Average test accuracy across clients unseen at training (train accuracy between parentheses).

Dataset	FedAvg	FedAvg+	ClusteredFL	Ditto	FedRep	APFL	pFedGP	kNN-Per (Ours)
FEMNIST	83.1 (83.3)	84.2 (88.5)	83.2 (86.0)	83.9 (86.9)	85.4 (88.9)	84.2 (85.5)	–	**88.1** (90.5)
CIFAR-10	72.9 (72.8)	75.3 (78.2)	73.9 (76.2)	79.7 (84.3)	76.4 (79.5)	79.2 (80.6)	–	**82.4** (87.1)
CIFAR-10 (v2)	67.5 (68.1)	85.1 (85.0)	79.6 (79.9)	85.9 (86.0)	89.0 (89.1)	82.3 (82.5)	89.0 (88.8)	**93.0** (93.1)
CIFAR-100	47.1 (47.5)	50.8 (53.4)	47.1 (48.2)	52.1 (57.3)	53.5 (58.2)	49.1 (52.7)	–	**56.1** (59.3)
CIFAR-100 (v2)	42.1 (42.2)	47.9 (48.1)	43.2 (43.4)	48.8 (48.5)	69.8 (70.0)	48.2 (48.4)	61.3 (61.0)	**74.3** (74.5)
Shakespeare	49.0 (48.3)	49.3 (48.1)	49.4 (46.7)	48.1 (49.2)	48.7 (47.8)	46.1 (52.7)	–	**50.7** (64.2)

6. Experiments

Average performance of personalized models. The performance of each personalized model (which coincides with the global one in the case of FedAvg) is evaluated on the local test dataset (unseen at training). Table 2 shows the average weighted accuracy with weights proportional to local dataset sizes. kNN-Per consistently achieves the highest accuracy across all datasets. We observe that Local performs much worse than any other FL method as expected (e.g., 25 pp w.r.t. kNN-Per or 22 pp w.r.t. to Ditto on CIFAR-10). Local outperforms some other FL methods on CIFAR-10/100 (v2). This splitting was proposed in pFedGP's paper—where the same result is observed (Achituve et al., 2021, Table 1). This occurs because each client only receives samples for a few classes, and then its local task is much easier than the global one.

Fairness across clients. Table 2 also shows the bottom decile of the accuracy of personalized models, i.e., the $(M/10)$-th worst accuracy (the minimum accuracy is particularly noisy, notably because some local test datasets are very small). We observe that even clients with the worst personalized models are still better off when kNN-Per is used for training.

Generalization to unseen clients. An advantage of kNN-Per is that a "new" client arriving after training may easily learn a personalized model: it may simply retrieve the global model (whose training it did not participate to) from the orchestrator and use it to build the local datastore for kNN. Even if this scenario was not explicitly considered in their original papers, other personalized FL methods can also be adapted to new clients as follows. FedAvg+ personalizes the global model through stochastic gradient updates on the new client's local dataset. Ditto operates similarly, but maintains a penalization term proportional to the distance between the personalized model and the global model. FedRep trains the network head using the local dataset, while freezing the body as in the global model. For pFedGP new clients inherit the previously trained shared network and compute their local kernel. ClusteredFL assigns the new client to one learned cluster model using a held-out validation set. In the case of FedAvg, there is no personalization and the new client uses directly the global model. We performed an experiment where only 80% of the clients participated to the training and the remaining 20% joined later. Results in Table 3 show that, despite its simplicity in dealing with new clients, kNN-Per still outperforms all other methods.

Effect of local dataset's size. Beside its relevance for some practical scenarios, the distinction between old and new clients also helps us to evaluate how different factors contribute to the final performance of kNN-Per. For example, to understand how the size of the local dataset affects performance, we reduced proportionally the size of new clients' local datasets, while maintaining unchanged the global model, which was trained on old clients. Figure 1 shows that new clients still reap most of kNN-Per's benefits even if their local datastore is reduced by a factor 3. Note that if we had changed the local dataset sizes also for old clients, the global model (and then the representation) would have changed too, making it difficult to isolate the effect of the local datastore size. We show the results for

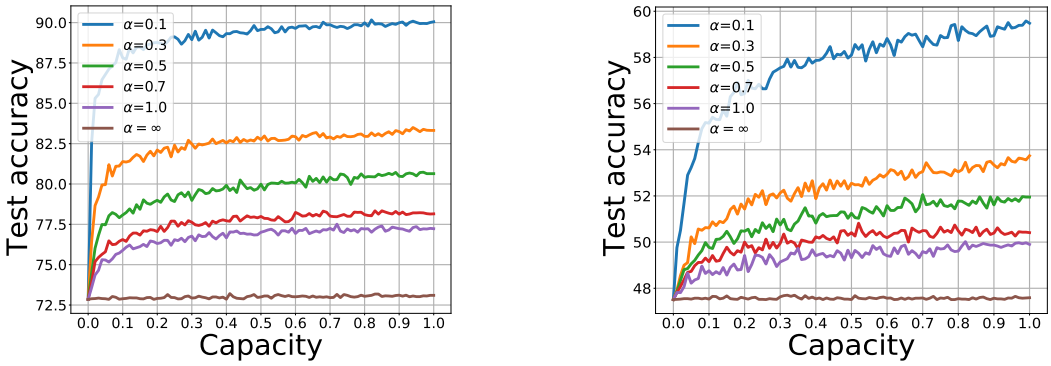

(a) CIFAR-10 (b) CIFAR-100

Figure 1. Test accuracy vs capacity (local datastore size). The capacity is normalized with respect to the initial size of the client's dataset partition. Smaller values of α correspond to more heterogeneous data distributions across clients.

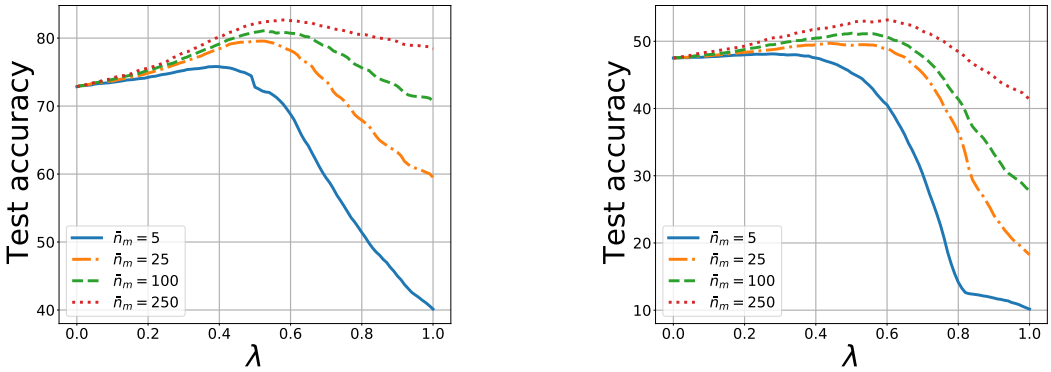

(a) CIFAR-10 (b) CIFAR-100

Figure 2. Test accuracy vs the interpolation parameter λ (shared across clients) for different average local dataset sizes. For $\lambda = 1$ (resp. $\lambda = 0$) the client uses only the kNN model (resp. the global model).

this experiment in Figure 6 (Appendix B).

Effect of data heterogeneity. Figure 1 also shows that, as expected by Theorem 4.1, the benefit of the memorization mechanism is larger when data distributions are more heterogeneous (smaller α). While other methods also benefit from higher heterogeneity, `kNN-Per` appears to address statistical heterogeneity more effectively (Figure 10). Note that if local distributions were identical ($\alpha \to \infty$), no personalization method would provide any advantage.

Hyperparameters. `kNN-Per`'s performance is not highly sensitive to the value k which can be selected between 7 and 14 for CIFAR-10 and between 5 and 12 for CIFAR-100 with less than 0.2 percentage points of accuracy variation (see Figure 5 in Appendix B). Similarly, scaling the Euclidean distance by a factor σ has almost no effect for values of σ between 0.1 and 100 and between 1 and 100, respectively for CIFAR-10 and CIFAR-100 (see Figure 7 in Appendix B). The interpolation parameter λ_m plays a more important role. Experiments in Appendix B (Figure 8) show that, as expected, the larger the local dataset, the more clients rely on the local kNN model. Interestingly, clients give a larger weight to the kNN model than to the global one ($\lambda > 1/2$) for datasets with just one hundred samples (Figure 2).

Effect of global model's quality. Assumption 4 stipulates that the smaller the expected loss of the global model, the better representations' distances capture the variability of $\mathbf{x} \mapsto \mathcal{D}_m(\cdot|\mathbf{x})$ and then the more accurate the kNN model. This effect is quantified by Lemma A.2, where the loss of the local memorization mechanism is upper bounded by a term that depends linearly on the loss of the global model. In order to validate this assumption, we study the relation between the test accuracies of the global model and `kNN-Per`. In particular, we trained a global model for CIFAR-10, in a centralized way, and we save the weights at different stages of the training, leading to global models with different accuracy. Figure 3 shows the test accuracy of `kNN-Per` with $\lambda = 1$ (i.e., when only the kNN predictor is used) as a func-

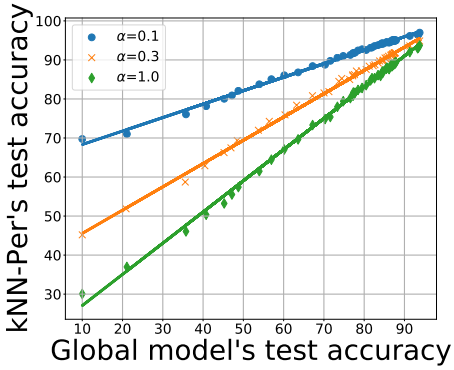

Figure 3. Effect of the global model's quality on the test accuracy of `kNN-Per` with $\lambda = 1$. CIFAR-10.

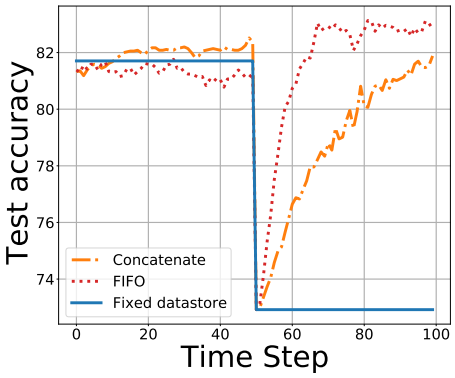

Figure 4. Effect of the global model's quality on the test accuracy of `kNN-Per` with $\lambda = 1$. CIFAR-10.

tion of the global model's test accuracy for different levels of heterogeneity. We observe that, quite unexpectedly, the relation between the two accuracies is almost linear. Additional experiments (also including CIFAR-100) in Appendix B confirm these findings.

Robustness to distribution shift. `kNN-Per` offers a simple and effective way to address statistical heterogeneity in a dynamic environment where client's data distributions change after training. We simulate such a dynamic environment as follows. Client m initially has a datastore with instances sampled from data distribution $\mathcal{D}_m$. At each time step $t < t_0$, client m receives a batch of instances drawn from $\mathcal{D}_m$. At time step t_0, a data distribution shift takes place, i.e., for $t_0 \leq t \leq T$, client m receives instances drawn from a data distribution $\mathcal{D}'_m \neq \mathcal{D}_m$. Upon receiving new instances, client m may use those instances to update its datastore. We consider 3 different strategies: (1) *first-in-first-out* (FIFO) where, at time step t, new instances replace the oldest ones; (2) *concatenate*, where the new samples are simply added to the datastore; (3) *fixed datastore*, where the datastore is not updated at all. Figure 4 shows the evaluation of the test accuracy across time. If clients do not update their datastores, there is a significant drop in accuracy as soon as the distribution changes at $t_0 = 50$. Under FIFO, we observe some random fluctuations for the accuracy for $t < t_0$, as repository changes affect the kNN predictions. While accuracy inevitably drops for $t = t_0$, it then increases as datastores are progressively populated by instances from the new distributions. Under the "concatenate" strategy, results are similar, but 1) accuracy increases for $t < t_0$ as the quality of kNN predictors improves for larger datastores, 2) accuracy increases also for $t > t_0$, but at a slower pace than what observed under FIFO, as samples from the old distribution are never evicted. Experiments' details and results for CIFAR-100 are in Appendix B.

Appendix B also includes experiments to evaluate the effect of system heterogeneity and the possibility to use aggressive nearest neighbours compression techniques like `ProtoNN` (Gupta et al., 2017).

7. Conclusion

In this paper, we showed that local memorization at each client is a simple and effective way to address statistical heterogeneity in federated learning. In particular, while a global model trained with classic FL techniques, like `FedAvg`, may not deliver accurate predictions at each client, it may still provide a good representation of the input, which can be advantageously used by a local kNN model. This finding suggests that combining memorization techniques with neural networks has additional benefits other than those highlighted in the seminal papers (Grefenstette et al., 2015; Joulin and Mikolov, 2015) and the recent applications to natural language processing (Khandelwal et al., 2019; 2020).

The better performance of `kNN-Per` in comparison to `FedRep` and `pFedGP` show that jointly learning the shared representation and the local models (as `FedRep` and `pFedGP` do) may lead to potentially conflicting and interfering goals, but further study is required to understand this interaction. Semi-parametric learning (Bickel et al., 1993) could be the right framework to formalize this problem, but its extension to a federated setting is still unexplored.

Acknowledgments

This work has been supported by the French government, through the 3IA Côte d'Azur Investments in the Future project managed by the National Research Agency (ANR) with the reference number ANR-19-P3IA-0002. The authors are grateful to the OPAL infrastructure from Université Côte d'Azur for providing computational resources and technical support.

References

Tian Li, Anit Kumar Sahu, Ameet Talwalkar, and Virginia Smith. Federated learning: Challenges, methods, and future directions. *IEEE Signal Processing Magazine*, 37 (3):50–60, 2020.

Peter Kairouz, H Brendan McMahan, Brendan Avent, Aurélien Bellet, Mehdi Bennis, Arjun Nitin Bhagoji, Keith Bonawitz, Zachary Charles, Graham Cormode, Rachel Cummings, et al. Advances and open problems in federated learning. *arXiv preprint arXiv:1912.04977*, 2019.

Brendan McMahan, Eider Moore, Daniel Ramage, Seth Hampson, and Blaise Aguera y Arcas. Communication-efficient learning of deep networks from decentralized data. In *Artificial Intelligence and Statistics*, pages 1273–1282. PMLR, 2017.

Jakub Konečny, H Brendan McMahan, Felix X Yu, Peter Richtárik, Ananda Theertha Suresh, and Dave Bacon. Federated learning: Strategies for improving communication efficiency. *arXiv preprint arXiv:1610.05492*, 2016.

Anit Kumar Sahu, Tian Li, Maziar Sanjabi, M. Zaheer, Ameet S. Talwalkar, and Virginia Smith. On the convergence of federated optimization in heterogeneous networks. *ArXiv*, abs/1812.06127, 2018.

Sai Praneeth Karimireddy, Satyen Kale, Mehryar Mohri, Sashank Reddi, Sebastian Stich, and Ananda Theertha Suresh. Scaffold: Stochastic controlled averaging for federated learning. In *International Conference on Machine Learning*, pages 5132–5143. PMLR, 2020.

Mehryar Mohri, Gary Sivek, and Ananda Theertha Suresh. Agnostic federated learning. In *International Conference on Machine Learning*, pages 4615–4625. PMLR, 2019.

Tian Li, Shengyuan Hu, Ahmad Beirami, and Virginia Smith. Ditto: Fair and robust federated learning through personalization. In *International Conference on Machine Learning*, pages 6357–6368. PMLR, 2021.

Urvashi Khandelwal, Omer Levy, Dan Jurafsky, Luke Zettlemoyer, and Mike Lewis. Generalization through memorization: Nearest neighbor language models. In *International Conference on Learning Representations*, 2019.

Urvashi Khandelwal, Angela Fan, Dan Jurafsky, Luke Zettlemoyer, and Mike Lewis. Nearest neighbor machine translation. *arXiv preprint arXiv:2010.00710*, 2020.

Nicolas Papernot and Patrick McDaniel. Deep k-nearest neighbors: Towards confident, interpretable and robust deep learning. *arXiv preprint arXiv:1803.04765*, 2018.

Emin Orhan. A simple cache model for image recognition. *Advances in Neural Information Processing Systems*, 31, 2018.

Jake Snell, Kevin Swersky, and Richard Zemel. Prototypical networks for few-shot learning. *Advances in neural information processing systems*, 30, 2017.

Yan Wang, Wei-Lun Chao, Kilian Q Weinberger, and Laurens van der Maaten. Simpleshot: Revisiting nearest-neighbor classification for few-shot learning. *arXiv preprint arXiv:1911.04623*, 2019.

Yihan Jiang, Jakub Konečnỳ, Keith Rush, and Sreeram Kannan. Improving federated learning personalization via model agnostic meta learning. *arXiv preprint arXiv:1909.12488*, 2019.

Tao Yu, Eugene Bagdasaryan, and Vitaly Shmatikov. Salvaging federated learning by local adaptation. *arXiv preprint arXiv:2002.04758*, 2020.

Hong-You Chen and Wei-Lun Chao. On bridging generic and personalized federated learning for image classification. In *International Conference on Learning Representations*, 2022. URL https://openreview.net/forum?id=I1hQbx10Kxn.

Gary Cheng, Karan Chadha, and John Duchi. Finetuning is fine in federated learning. *arXiv preprint arXiv:2108.07313*, 2021.

Mikhail Khodak, Maria-Florina F Balcan, and Ameet S Talwalkar. Adaptive gradient-based meta-learning methods. In *Advances in Neural Information Processing Systems*, pages 5917–5928, 2019.

Alireza Fallah, Aryan Mokhtari, and Asuman Ozdaglar. Personalized federated learning with theoretical guarantees: A model-agnostic meta-learning approach. In H. Larochelle, M. Ranzato, R. Hadsell, M. F. Balcan, and H. Lin, editors, *Advances in Neural Information Processing Systems*, volume 33, pages 3557–3568. Curran Associates, Inc., 2020. URL https://proceedings.neurips.cc/paper/2020/file/24389bfe4fe2eba8bf9aa9203a44cdad-Paper.pdf.

Durmus Alp Emre Acar, Yue Zhao, Ruizhao Zhu, Ramon Matas, Matthew Mattina, Paul Whatmough, and Venkatesh Saligrama. Debiasing model updates for improving personalized federated training. In Marina Meila and Tong Zhang, editors, *Proceedings of the 38th International Conference on Machine Learning*, volume 139 of *Proceedings of Machine Learning Research*, pages 21–31. PMLR, 7 2021. URL https://proceedings.mlr.press/v139/acar21a.html.

Felix Sattler, Klaus-Robert Müller, and Wojciech Samek. Clustered federated learning: Model-agnostic distributed multitask optimization under privacy constraints. *IEEE Transactions on Neural Networks and Learning Systems*, 2020.

Avishek Ghosh, Jichan Chung, Dong Yin, and Kannan Ramchandran. An efficient framework for clustered federated learning. In H. Larochelle, M. Ranzato, R. Hadsell, M. F. Balcan, and H. Lin, editors, *Advances in Neural Information Processing Systems*, volume 33, pages 19586–19597. Curran Associates, Inc., 2020. URL https://proceedings.neurips.cc/paper/2020/file/e32cc80bf07915058ce90722ee17bb71-Paper.pdf.

Yishay Mansour, Mehryar Mohri, Jae Ro, and Ananda Theertha Suresh. Three approaches for personalization with applications to federated learning. *arXiv preprint arXiv:2002.10619*, 2020.

Othmane Marfoq, Giovanni Neglia, Aurélien Bellet, Laetitia Kameni, and Richard Vidal. Federated multi-task learning under a mixture of distributions. *arXiv preprint arXiv:2108.10252*, 2021.

Virginia Smith, Chao-Kai Chiang, Maziar Sanjabi, and Ameet Talwalkar. Federated multi-task learning. In *Proceedings of the 31st International Conference on Neural Information Processing Systems*, NIPS'17, page 4427–4437, Red Hook, NY, USA, 2017. Curran Associates Inc. ISBN 9781510860964.

Paul Vanhaesebrouck, Aurélien Bellet, and Marc Tommasi. Decentralized Collaborative Learning of Personalized Models over Networks. In *AISTATS*, 2017.

Valentina Zantedeschi, Aurélien Bellet, and Marc Tommasi. Fully decentralized joint learning of personalized models and collaboration graphs. volume 108 of *Proceedings of Machine Learning Research*, pages 864–874, Online, 8 2020. PMLR. URL http://proceedings.mlr.press/v108/zantedeschi20a.html.

Filip Hanzely and Peter Richtárik. Federated learning of a mixture of global and local models, 2020.

Filip Hanzely, Slavomír Hanzely, Samuel Horváth, and Peter Richtarik. Lower bounds and optimal algorithms for personalized federated learning. In H. Larochelle, M. Ranzato, R. Hadsell, M. F. Balcan, and H. Lin, editors, *Advances in Neural Information Processing Systems*, volume 33, pages 2304–2315. Curran Associates, Inc., 2020. URL https://proceedings.neurips.cc/paper/2020/file/187acf7982f3c169b3075132380986e4-Paper.pdf.

Canh T. Dinh, Nguyen Tran, and Josh Nguyen. Personalized federated learning with moreau envelopes. In H. Larochelle, M. Ranzato, R. Hadsell, M. F. Balcan, and H. Lin, editors, *Advances in Neural Information Processing Systems*, volume 33, pages 21394–21405. Curran Associates, Inc., 2020. URL https://proceedings.neurips.cc/paper/2020/file/f4f1f13c8289ac1b1ee0ff176b56fc60-Paper.pdf.

Canh T Dinh, Tung T Vu, Nguyen H Tran, Minh N Dao, and Hongyu Zhang. Fedu: A unified framework for federated multi-task learning with laplacian regularization. *arXiv preprint arXiv:2102.07148*, 2021.

Yutao Huang, Lingyang Chu, Zirui Zhou, Lanjun Wang, Jiangchuan Liu, Jian Pei, and Yong Zhang. Personalized cross-silo federated learning on non-iid data. In *AAAI*, pages 7865–7873, 2021. URL https://ojs.aaai.org/index.php/AAAI/article/view/16960.

Yuyang Deng, Mohammad Mahdi Kamani, and Mehrdad Mahdavi. Adaptive personalized federated learning. *arXiv preprint arXiv:2003.13461*, 2020.

Luca Corinzia and Joachim M. Buhmann. Variational federated multi-task learning, 2019.

Michael Zhang, Karan Sapra, Sanja Fidler, Serena Yeung, and Jose M. Alvarez. Personalized federated learning with first order model optimization. In *International Conference on Learning Representations*, 2021. URL https://openreview.net/forum?id=ehJqJQk9cw.

Liam Collins, Hamed Hassani, Aryan Mokhtari, and Sanjay Shakkottai. Exploiting shared representations for personalized federated learning. In Marina Meila and Tong Zhang, editors, *Proceedings of the 38th International Conference on Machine Learning*, volume 139 of *Proceedings of Machine Learning Research*, pages 2089–2099. PMLR, 18–24 Jul 2021. URL https://proceedings.mlr.press/v139/collins21a.html.

Manoj Ghuhan Arivazhagan, V. Aggarwal, Aaditya Kumar Singh, and Sunav Choudhary. Federated learning with personalization layers. *ArXiv*, abs/1912.00818, 2019.

Idan Achituve, Aviv Shamsian, Aviv Navon, Gal Chechik, and Ethan Fetaya. Personalized federated learning with gaussian processes. *Advances in Neural Information Processing Systems*, 34, 2021.

Paul Pu Liang, Terrance Liu, Liu Ziyin, Nicholas B Allen, Randy P Auerbach, David Brent, Ruslan Salakhutdinov, and Louis-Philippe Morency. Think locally, act globally:

Federated learning with local and global representations. *arXiv preprint arXiv:2001.01523*, 2020.

Kang Wei, Jun Li, Ming Ding, Chuan Ma, Howard H. Yang, Farhad Farokhi, Shi Jin, Tony Q. S. Quek, and H. Vincent Poor. Federated learning with differential privacy: Algorithms and performance analysis. *IEEE Transactions on Information Forensics and Security*, 15:3454–3469, 2020. doi: 10.1109/TIFS.2020.2988575.

P.J. Bickel, C.A.J. Klaassen, Y. Ritov, and J.A. Wellner. *Efficient and Adaptive Estimation for Semiparametric Models*. Johns Hopkins series in the mathematical sciences. Springer New York, 1998. ISBN 9780387984735. URL https://books.google.fr/books?id=lSnTm6SC_SMC.

Tao Lin, Lingjing Kong, Sebastian U Stich, and Martin Jaggi. Ensemble distillation for robust model fusion in federated learning. In H. Larochelle, M. Ranzato, R. Hadsell, M. F. Balcan, and H. Lin, editors, *Advances in Neural Information Processing Systems*, volume 33, pages 2351–2363. Curran Associates, Inc., 2020. URL https://proceedings.neurips.cc/paper/2020/file/18df51b97ccd68128e994804f3eccc87-Paper.pdf.

Daliang Li and Junpu Wang. Fedmd: Heterogenous federated learning via model distillation. *arXiv preprint arXiv:1910.03581*, 2019.

Zhuangdi Zhu, Junyuan Hong, and Jiayu Zhou. Data-free knowledge distillation for heterogeneous federated learning. In Marina Meila and Tong Zhang, editors, *Proceedings of the 38th International Conference on Machine Learning*, volume 139 of *Proceedings of Machine Learning Research*, pages 12878–12889. PMLR, 18–24 Jul 2021. URL https://proceedings.mlr.press/v139/zhu21b.html.

Lan Zhang and Xiaoyong Yuan. Fedzkt: Zero-shot knowledge transfer towards heterogeneous on-device models in federated learning. *arXiv preprint arXiv:2109.03775*, 2021.

Enmao Diao, Jie Ding, and Vahid Tarokh. Heterofl: Computation and communication efficient federated learning for heterogeneous clients. In *International Conference on Learning Representations*, 2020.

Samuel Horváth, Stefanos Laskaridis, Mario Almeida, Ilias Leontiadis, Stylianos Venieris, and Nicholas Donald Lane. FjORD: Fair and accurate federated learning under heterogeneous targets with ordered dropout. In A. Beygelzimer, Y. Dauphin, P. Liang, and J. Wortman Vaughan, editors, *Advances in Neural Information Processing Systems*, 2021. URL https://openreview.net/forum?id=4fLr7H5D_eT.

Amaury Bouchra Pilet, Davide Frey, and François Taïani. Simple, efficient and convenient decentralized multi-task learning for neural networks. In *IDA*, pages 37–49, 2021.

Yue Tan, Guodong Long, Lu Liu, Tianyi Zhou, Qinghua Lu, Jing Jiang, and Chengqi Zhang. FedProto: Federated Prototype Learning across Heterogeneous Clients. In *AAAI Conference on Artificial Intelligence*, 2022.

Aviv Shamsian, Aviv Navon, Ethan Fetaya, and Gal Chechik. Personalized federated learning using hypernetworks. In *ICML*, 2021.

Jeff Johnson, Matthijs Douze, and Herve Jegou. Billion-scale similarity search with gpus. *IEEE Transactions on Big Data*, pages 1–1, 2019.

Yu A Malkov and DA Yashunin. Efficient and robust approximate nearest neighbor search using hierarchical navigable small world graphs. *IEEE Transactions on Pattern Analysis and Machine Intelligence*, 42(4):824–836, 2020.

Chirag Gupta, Arun Sai Suggala, Ankit Goyal, Harsha Vardhan Simhadri, Bhargavi Paranjape, Ashish Kumar, Saurabh Goyal, Raghavendra Udupa, Manik Varma, and Prateek Jain. ProtoNN: Compressed and accurate kNN for resource-scarce devices. In Doina Precup and Yee Whye Teh, editors, *Proceedings of the 34th International Conference on Machine Learning*, volume 70 of *Proceedings of Machine Learning Research*, pages 1331–1340. PMLR, 06–11 Aug 2017. URL https://proceedings.mlr.press/v70/gupta17a.html.

Aurélien Bellet, Amaury Habrard, and Marc Sebban. *Metric Learning*, volume 9 of *Synthesis Lectures on Artificial Intelligence and Machine Learning*. Morgan & Claypool Publishers (USA), Synthesis Lectures on Artificial Intelligence and Machine Learning, pp 1-151, January 2015. doi: 10.2200/S00626ED1V01Y201501AIM030. URL https://hal.archives-ouvertes.fr/hal-01121733.

Shai Shalev-Shwartz and Shai Ben-David. *Understanding machine learning: From theory to algorithms*. Cambridge university press, 2014.

Sebastian Caldas, Sai Meher Karthik Duddu, Peter Wu, Tian Li, Jakub Konečnỳ, H Brendan McMahan, Virginia Smith, and Ameet Talwalkar. Leaf: A benchmark for federated settings. *arXiv preprint arXiv:1812.01097*, 2018.

Alex Krizhevsky. Learning multiple layers of features from tiny images. Technical report, 2009.

Hongyi Wang, Mikhail Yurochkin, Yuekai Sun, Dimitris Papailiopoulos, and Yasaman Khazaeni. Federated learning with matched averaging. In *International Conference on Learning Representations*, 2020. URL https://openreview.net/forum?id=BkluqlSFDS.

Wei Li and Andrew McCallum. Pachinko allocation: Dag-structured mixture models of topic correlations. In *Proceedings of the 23rd International Conference on Machine Learning*, ICML '06, page 577–584, New York, NY, USA, 2006. Association for Computing Machinery. ISBN 1595933832. doi: 10.1145/1143844.1143917. URL https://doi.org/10.1145/1143844.1143917.

Sashank J. Reddi, Zachary Charles, Manzil Zaheer, Zachary Garrett, Keith Rush, Jakub Konečný, Sanjiv Kumar, and Hugh Brendan McMahan. Adaptive federated optimization. In *International Conference on Learning Representations*, 2021. URL https://openreview.net/forum?id=LkFG3lB13U5.

Mark Sandler, Andrew Howard, Menglong Zhu, Andrey Zhmoginov, and Liang-Chieh Chen. Mobilenetv2: Inverted residuals and linear bottlenecks. In *Proceedings of the IEEE conference on computer vision and pattern recognition*, pages 4510–4520, 2018.

Edward Grefenstette, Karl Moritz Hermann, Mustafa Suleyman, and Phil Blunsom. Learning to transduce with unbounded memory. In *NIPS*, NIPS'15, pages 1828–1836, Cambridge, MA, USA, 2015. MIT Press. URL http://dl.acm.org/citation.cfm?id=2969442.2969444.

Armand Joulin and Tomas Mikolov. Inferring algorithmic patterns with stack-augmented recurrent nets. In *NIPS*, NIPS'15, pages 190–198, Cambridge, MA, USA, 2015. MIT Press. URL http://dl.acm.org/citation.cfm?id=2969239.2969261.

Peter J Bickel, Chris AJ Klaassen, Peter J Bickel, Ya'acov Ritov, J Klaassen, Jon A Wellner, and YA'Acov Ritov. *Efficient and adaptive estimation for semiparametric models*, volume 4. Johns Hopkins University Press Baltimore, 1993.

A. Proofs

In the general description of `kNN-Per`, and in our experiments, we considered that each client $m \in [M]$ uses its whole dataset $\mathcal{S}_m$ both to train the base shared model $h_{\mathcal{S}}$—and the corresponding representation function $\phi_{h_{\mathcal{S}}}$—and to populate the local datastore.

In the analysis, for simplicity, we deviate by this operation and consider that each local dataset $\mathcal{S}_m$ is split in two disjoint parts ($\mathcal{S}_m = \mathcal{S}'_m \dot{\bigcup} \mathcal{S}''_m$), with $\mathcal{S}'_m$ used to train the base model and $\mathcal{S}''_m$ used to populate the local datastore. Moreover, we assume that the two parts have the same size, i.e., $n'_m = n''_m = n_m/2$ for all $m \in [M]$, where n'_m and n''_m denote the size of $\mathcal{S}'_m$ and $\mathcal{S}''_m$, respectively. In general, the result holds if the two parts have a fixed relative size across clients (i.e., $n'_{m_1}/n_{m_1} = n'_{m_2}/n_{m_2}$ for all m_1 and m_2 in $[m]$).

Let $\mathcal{S}'$ denote the whole data used to train the base model, i.e., $\mathcal{S}' = \bigcup_{m\in[M]} \mathcal{S}'_m$. We observe that the base model $h_{\mathcal{S}}$ is only function of $\mathcal{S}'$, and then we can write $h_{\mathcal{S}'}$. Instead, the local model $h^{(1)}_{\mathcal{S}_m}$ is both a function of $\mathcal{S}'$ (used to learn the shared representation $\phi'_{\mathcal{S}}$) and of $\mathcal{S}''_m$ (used to populate the datastore). In order to stress such dependence, we then write $h^{(1)}_{\mathcal{S}''_m,\mathcal{S}'}$.

A.1. Proof of Theorem 4.1

Theorem 4.1. *Suppose that Assumptions 1–4 hold, and consider $m \in [M]$ and $\lambda_m \in (0,1)$, then there exist constants c_1, c_2, c_3, c_4, and $c_5 \in \mathbb{R}$, such that*

$$\begin{aligned}\mathop{\mathbb{E}}_{\mathcal{S}\sim\otimes_{m=1}^{M}\mathcal{D}_m^{n_m}} \left[\mathcal{L}_{\mathcal{D}_m}\left(h_{m,\lambda_m}\right)\right] \leq{}& (1+\lambda_m)\cdot\mathcal{L}_{\mathcal{D}_m}\left(h^*_m\right) + c_1\left(1-\lambda_m\right)\cdot\left(\mathrm{disc}_{\mathcal{H}}\left(\bar{\mathcal{D}},\mathcal{D}_m\right)+1\right)\\ &+ c_2\lambda_m\cdot\frac{\sqrt{p}}{\sqrt[p+1]{n_m}}\cdot\mathrm{disc}_{\mathcal{H}}\left(\bar{\mathcal{D}},\mathcal{D}_m\right) + c_3\left(1-\lambda_m\right)\cdot\sqrt{\frac{d_{\mathcal{H}}}{n}}\cdot\sqrt{c_4+\log\left(\frac{n}{d_{\mathcal{H}}}\right)}\\ &+ c_5\lambda_m\cdot\sqrt{\frac{d_{\mathcal{H}}}{n}}\cdot\sqrt{c_4+\log\left(\frac{n}{d_{\mathcal{H}}}\right)}\cdot\frac{\sqrt{p}}{\sqrt[p+1]{n_m}},\end{aligned} \tag{14}$$

where $d_{\mathcal{H}}$ is the the VC dimension of the hypothesis class $\mathcal{H}$, $n = \sum_{m=1}^{M} n_m$, $\bar{\mathcal{D}} = \sum_{m=1}^{M} \frac{n_m}{n}\cdot\mathcal{D}_m$, p is the dimension of representations, and disc_H is the label discrepancy associated to the hypothesis class $\mathcal{H}$.

Proof. The idea of the proof is to bound both the expected error of the *shared* base model (Lemma A.1) and the error of the local kNN retrieval mechanism (Lemma A.2) before using the convexity of the loss function to bound the error of h_{m,λ_m}.

Consider $\mathcal{S} \sim \otimes_{m=1}^{M}\mathcal{D}_m^{n_m}$ or, equivalently, $\mathcal{S} = \mathcal{S}' \cup \mathcal{S}''$, where $\mathcal{S}' \sim \otimes_{m=1}^{M}\mathcal{D}_m^{n_m/2}$, and $\mathcal{S}'' = \cup_{m\in[M]}\mathcal{S}''_m$ and $\mathcal{S}''_m \sim \mathcal{D}_m^{n_m/2}$.

For $m \in [M]$, and $\lambda_m \in (0,1)$, we have

$$h_{m,\lambda_m} = \lambda_m\cdot h^{(1)}_{\mathcal{S}''_m,\mathcal{S}'} + (1-\lambda_m)\cdot h_{\mathcal{S}'}. \tag{15}$$

From Assumption 3 and the linearity of the expectation, it follows

$$\mathcal{L}_{\mathcal{D}_m}\left(h_{m,\lambda_m}\right) \leq \lambda_m\cdot\mathcal{L}_{\mathcal{D}_m}\left(h^{(1)}_{\mathcal{S}''_m,\mathcal{S}'}\right) + (1-\lambda_m)\cdot\mathcal{L}_{\mathcal{D}_m}\left(h_{\mathcal{S}'}\right). \tag{16}$$

Using Lemma A.2 and Lemma A.1, and applying expectation over samples $\mathcal{S} \sim \otimes_{m=1}^{M} \mathcal{D}_m^{n_m}$, we have

$$\begin{aligned}
\mathop{\mathbb{E}}_{\mathcal{S}\sim\otimes_{m=1}^{M}\mathcal{D}_m^{n_m}} \left[\mathcal{L}_{\mathcal{D}_m}\left(h_{m,\lambda_m}\right)\right] &\leq \lambda_m \cdot \mathop{\mathbb{E}}_{\mathcal{S}'\sim\otimes_{m=1}^{M}\mathcal{D}_m^{n_m/2}} \left[\mathop{\mathbb{E}}_{\mathcal{S}''\sim\otimes_{m=1}^{M}\mathcal{D}_m^{n_m/2}} \left[\mathcal{L}_{\mathcal{D}_m}\left(h^{(1)}_{\mathcal{S}''_m,\mathcal{S}'}\right)\right]\right] \\
&\quad + (1-\lambda_m) \cdot \mathop{\mathbb{E}}_{\mathcal{S}'\sim\otimes_{m=1}^{M}\mathcal{D}_m^{n_m/2}} \left[\mathop{\mathbb{E}}_{\mathcal{S}''\sim\otimes_{m=1}^{M}\mathcal{D}_m^{n_m/2}} \left[\mathcal{L}_{\mathcal{D}_m}\left(h_{\mathcal{S}'}\right)\right]\right] \qquad (17) \\
&\leq 2\lambda_m \mathcal{L}_{\mathcal{D}_m}\left(h_m^*\right) + 6\lambda_m\gamma_1 \frac{\sqrt{p}}{\sqrt[p+1]{n_m}} \\
&\quad + 6\lambda_m\gamma_2 \frac{\sqrt{p}}{\sqrt[p+1]{n_m}} \cdot \left(\mathop{\mathbb{E}}_{\mathcal{S}'\sim\otimes_{m=1}^{M}\mathcal{D}_m^{n_m/2}} \left[\mathcal{L}_{\mathcal{D}_m}\left(h_{\mathcal{S}'}\right)\right] - \mathcal{L}_{\mathcal{D}_m}\left(h_m^*\right)\right) \\
&\quad + (1-\lambda_m) \cdot \mathop{\mathbb{E}}_{\mathcal{S}'\sim\otimes_{m=1}^{M}\mathcal{D}_m^{n_m/2}} \left[\mathcal{L}_{\mathcal{D}_m}\left(h_{\mathcal{S}'}\right)\right] \qquad (18) \\
&\leq 2\lambda_m \mathcal{L}_{\mathcal{D}_m}\left(h_m^*\right) + 6\lambda_m\gamma_1 \frac{\sqrt{p}}{\sqrt[p+1]{n_m}} \\
&\quad + 6\lambda_m\gamma_2 \frac{\sqrt{p}}{\sqrt[p+1]{n_m}} \cdot \left(\delta_1 \cdot \sqrt{\frac{d_{\mathcal{H}}}{n}} \cdot \sqrt{\delta_2 + \log\left(\frac{n}{d_{\mathcal{H}}}\right)} + 2 \cdot \mathrm{disc}_{\mathcal{H}}\left(\bar{\mathcal{D}}, \mathcal{D}_m\right)\right) \\
&\quad + (1-\lambda_m) \cdot \left(\mathcal{L}_{\mathcal{D}_m}\left(h_m^*\right) + \delta_1 \cdot \sqrt{\frac{d_{\mathcal{H}}}{n}} \cdot \sqrt{\delta_2 + \log\left(\frac{n}{d_{\mathcal{H}}}\right)} + 2 \cdot \mathrm{disc}_{\mathcal{H}}\left(\bar{\mathcal{D}}, \mathcal{D}_m\right)\right) \qquad (19) \\
&= (1+\lambda_m)\mathcal{L}_{\mathcal{D}_m}\left(h_m^*\right) + 6\lambda_m\gamma_1 \frac{\sqrt{p}}{\sqrt[p+1]{n_m}} \\
&\quad + 6\lambda_m\gamma_2 \frac{\sqrt{p}}{\sqrt[p+1]{n_m}} \delta_1 \cdot \sqrt{\frac{d_{\mathcal{H}}}{n}} \cdot \sqrt{\delta_2 + \log\left(\frac{n}{d_{\mathcal{H}}}\right)} + 12\lambda_m\gamma_2 \frac{\sqrt{p}}{\sqrt[p+1]{n_m}} \cdot \mathrm{disc}_{\mathcal{H}}\left(\bar{\mathcal{D}}, \mathcal{D}_m\right) \\
&\quad + \delta_1(1-\lambda_m) \cdot \sqrt{\frac{d_{\mathcal{H}}}{n}} \cdot \sqrt{\delta_2 + \log\left(\frac{n}{d_{\mathcal{H}}}\right)} + 2 \cdot (1-\lambda_m)\,\mathrm{disc}_{\mathcal{H}}\left(\bar{\mathcal{D}}, \mathcal{D}_m\right). \qquad (20)
\end{aligned}$$

Rearranging the terms and taking $c_1 \triangleq 2$, $c_2 \triangleq \max\{12\gamma_2, 6\gamma_1\}$, $c_3 \triangleq \delta_1$, $c_4 \triangleq \delta_2$ and $c_5 \triangleq 6\gamma_2\delta_1$, the final result follows. □

A.2. Intermediate Lemmas

Lemma A.1. *Consider $m \in [M]$, then there exists constants $\delta_1, \delta_2 \in \mathbb{R}$ such that*

$$\mathop{\mathbb{E}}_{\mathcal{S}'\sim\otimes_{m=1}^{M}\mathcal{D}_m^{n_m/2}} \left[\mathcal{L}_{\mathcal{D}_m}\left(h_{\mathcal{S}'}\right)\right] \leq \mathcal{L}_{\mathcal{D}_m}\left(h_m^*\right) + \delta_1 \cdot \sqrt{\frac{d_{\mathcal{H}}}{n}} \cdot \sqrt{\delta_2 + \log\left(\frac{n}{d_{\mathcal{H}}}\right)} + 2 \cdot \mathrm{disc}_{\mathcal{H}}\left(\bar{\mathcal{D}}, \mathcal{D}_m\right), \qquad (21)$$

where d is the VC dimension of the hypothesis class $\mathcal{H}$, $\bar{\mathcal{D}} = \sum_{m=1}^{M} \frac{n_m}{n} \cdot \mathcal{D}_m$ and disc_H is the label discrepancy associated to the hypothesis class $\mathcal{H}$.

Proof. We remind that the label discrepancy associated to the hypothesis class $\mathcal{H}$ for two distributions $\mathcal{D}_1$ and $\mathcal{D}_2$ over features and labels is defined as (Mansour et al., 2020):

$$\mathrm{disc}_{\mathcal{H}}\left(\mathcal{D}_1, \mathcal{D}_2\right) = \max_{h\in\mathcal{H}} \left|\mathcal{L}_{\mathcal{D}_1}\left(h\right) - \mathcal{L}_{\mathcal{D}_2}\left(h\right)\right|. \qquad (22)$$

Consider $m \in [M]$ and $h^* \in \arg\min_{h\in\mathcal{H}} \mathcal{L}_{\bar{\mathcal{D}}}(h)$. For $\mathcal{S}' \sim \otimes_{m=1}^{M} \mathcal{D}_m^{n_m/2}$, we have

$$
\begin{aligned}
&\mathcal{L}_{\mathcal{D}_m}(h_{\mathcal{S}'}) - \mathcal{L}_{\mathcal{D}_m}(h_m^*) \\
&\quad = \mathcal{L}_{\mathcal{D}_m}(h_{\mathcal{S}'}) - \mathcal{L}_{\bar{\mathcal{D}}}(h_{\mathcal{S}'}) + \mathcal{L}_{\bar{\mathcal{D}}}(h_{\mathcal{S}'}) - \mathcal{L}_{\bar{\mathcal{D}}}(h_m^*) + \mathcal{L}_{\bar{\mathcal{D}}}(h_m^*) - \mathcal{L}_{\bar{\mathcal{D}}}(h^*) + \mathcal{L}_{\bar{\mathcal{D}}}(h^*) - \mathcal{L}_{\mathcal{D}_m}(h_m^*) && (23)\\
&\quad = \underbrace{\mathcal{L}_{\mathcal{D}_m}(h_{\mathcal{S}'}) - \mathcal{L}_{\bar{\mathcal{D}}}(h_{\mathcal{S}'})}_{\leq \mathrm{disc}_{\mathcal{H}}(\mathcal{D}_m,\bar{\mathcal{D}})} + \underbrace{\mathcal{L}_{\bar{\mathcal{D}}}(h_m^*) - \mathcal{L}_{\mathcal{D}_m}(h_m^*)}_{\leq \mathrm{disc}_{\mathcal{H}}(\mathcal{D}_m,\bar{\mathcal{D}})} + \underbrace{\mathcal{L}_{\bar{\mathcal{D}}}(h^*) - \mathcal{L}_{\bar{\mathcal{D}}}(h_m^*)}_{\leq 0} + \mathcal{L}_{\bar{\mathcal{D}}}(h_{\mathcal{S}'}) - \mathcal{L}_{\bar{\mathcal{D}}}(h^*) && (24)\\
&\quad \leq 2\cdot \mathrm{disc}_{\mathcal{H}}\left(\mathcal{D}_m,\bar{\mathcal{D}}\right) + \mathcal{L}_{\bar{\mathcal{D}}}(h_{\mathcal{S}'}) - \mathcal{L}_{\bar{\mathcal{D}}}(h^*) && (25)\\
&\quad = 2\cdot \mathrm{disc}_{\mathcal{H}}\left(\mathcal{D}_m,\bar{\mathcal{D}}\right) + \mathcal{L}_{\bar{\mathcal{D}}}(h_{\mathcal{S}'}) - \mathcal{L}_{\mathcal{S}'}(h_{\mathcal{S}'}) + \underbrace{\mathcal{L}_{\mathcal{S}'}(h_{\mathcal{S}'}) - \mathcal{L}_{\mathcal{S}'}(h^*)}_{\leq 0} + \mathcal{L}_{\mathcal{S}'}(h^*) - \mathcal{L}_{\bar{\mathcal{D}}}(h^*) && (26)\\
&\quad \leq 2\cdot \mathrm{disc}_{\mathcal{H}}\left(\mathcal{D}_m,\bar{\mathcal{D}}\right) + 2\cdot \sup_{h\in\mathcal{H}} \left|\mathcal{L}_{\bar{\mathcal{D}}}(h) - \mathcal{L}_{\mathcal{S}'}(h)\right|. && (27)
\end{aligned}
$$

We now bound $\mathbb{E}_{\mathcal{S}'\sim\otimes_{m=1}^{M}\mathcal{D}_m^{n_m/2}} \sup_{h\in\mathcal{H}} \left|\mathcal{L}_{\bar{\mathcal{D}}}(h) - \mathcal{L}_{\mathcal{S}'}(h)\right|$. We first observe that for every $h \in \mathcal{H}$, we can write $\mathcal{L}_{\bar{\mathcal{D}}}(h) = \mathbb{E}_{\mathcal{S}'\sim\otimes_{m=1}^{M}\mathcal{D}_m^{n_m/2}} \mathcal{L}_{\mathcal{S}'}(h)$. Therefore, despite the fact that the samples in $\mathcal{S}'$ are not i.i.d., we can follow the same steps as in the proof of Shalev-Shwartz and Ben-David (2014, Theorem 6.11), and conclude

$$
\mathop{\mathbb{E}}_{\mathcal{S}'\sim\otimes_{m=1}^{M}\mathcal{D}_m^{n_m/2}} \sup_{h\in\mathcal{H}} \left|\mathcal{L}_{\bar{\mathcal{D}}}(h) - \mathcal{L}_{\mathcal{S}'}(h)\right| \leq \frac{4 + \sqrt{\log\left(\tau_{\mathcal{H}}(n)\right)}}{\sqrt{n}}, \tag{28}
$$

where $\tau_{\mathcal{H}}$ is the growth function of class $\mathcal{H}$.

Let d denote the VC dimension of $\mathcal{H}$. From Sauer's lemma (Shalev-Shwartz and Ben-David, 2014, Lemma 6.10), we have that for $n > d+1$, $\tau_{\mathcal{H}}(n) \leq (en/d)^{d_{\mathcal{H}}}$. Therefore, there exist constants $\delta_1, \delta_2 \in \mathbb{R}$ (e.g., $\delta_1 = 4$, $\delta_2 = \max\{4/\sqrt{d_{\mathcal{H}}}, 1\}$), such that

$$
\mathop{\mathbb{E}}_{\mathcal{S}'\sim\otimes_{m=1}^{M}\mathcal{D}_m^{n_m/2}} \sup_{h\in\mathcal{H}} \left|\mathcal{L}_{\bar{\mathcal{D}}}(h) - \mathcal{L}_{\mathcal{S}'}(h)\right| \leq \frac{\delta_1}{2}\cdot\sqrt{\frac{d_{\mathcal{H}}}{n}}\cdot\sqrt{\delta_2 + \log\left(\frac{n}{d_{\mathcal{H}}}\right)}. \tag{29}
$$

Taking the expectation in Eq. (27) and using this inequality, we have

$$
\mathop{\mathbb{E}}_{\mathcal{S}'\sim\otimes_{m=1}^{M}\mathcal{D}_m^{n_m/2}} \left[\mathcal{L}_{\mathcal{D}_m}(h_{\mathcal{S}'})\right] \leq \mathcal{L}_{\mathcal{D}_m}(h_m^*) + \delta_1\cdot\sqrt{\frac{d_{\mathcal{H}}}{n}}\cdot\sqrt{\delta_2 + \log\left(\frac{n}{d_{\mathcal{H}}}\right)} + 2\cdot\mathrm{disc}_{\mathcal{H}}\left(\bar{\mathcal{D}},\mathcal{D}_m\right). \tag{30}
$$

□

The following Lemma proves an upper bound on the expected error of the 1-NN learning rule.

Lemma A.2 (Adapted from (Shalev-Shwartz and Ben-David, 2014, Thm 19.3))**.** *Under Assumptions 1, 2, and 4 for all $m \in [M]$, it holds*

$$
\mathop{\mathbb{E}}_{\mathcal{S}_m''\sim\mathcal{D}_m^{n_m/2}} \left[\mathcal{L}_{\mathcal{D}_m}\left(h^{(1)}_{\mathcal{S}_m'',\mathcal{S}'}\right)\right] \leq 2\mathcal{L}_{\mathcal{D}_m}(h_m^*) + 6\left\{\gamma_1 + \gamma_2\cdot\left[\mathcal{L}_{\mathcal{D}_m}(h_{\mathcal{S}'}) - \mathcal{L}_{\mathcal{D}_m}(h_m^*)\right]\right\}\cdot\frac{\sqrt{p}}{\sqrt[p+1]{n_m}}. \tag{31}
$$

Proof. Recall that for $m \in [M]$, the Bayes optimal rule, i.e., the hypothesis that minimizes $\mathcal{L}_{\mathcal{D}_m}(h)$ over all functions, is

$$
h_m^*(\mathbf{x}) = \mathbb{1}_{\{\eta_m(\mathbf{x})>1/2\}}. \tag{32}
$$

We note that the 1-NN rule can be expressed as follows:

$$
\left[h^{(1)}_{\mathcal{S}_m'',\mathcal{S}'}(\mathbf{x})\right]_y = \mathbb{1}_{\left\{y=\pi^{(1)}_{\mathcal{S}_m''}(\mathbf{x})\right\}}, \tag{33}
$$

where we are putting in evidence that the permutation π_m depends on the dataset $\mathcal{S}_m''$. Then, under Assumption 2, the loss function $l(\cdot)$ reduces to the 0-1 loss.

Consider samples $\mathcal{S} \sim \otimes_{m=1}^{M} \mathcal{D}_m^{n_m}$. Using Assumptions 1, 2 and 4, and following the same steps as in (Shalev-Shwartz and Ben-David, 2014, Lemma 19.1), we have

$$\mathop{\mathbb{E}}_{\mathcal{S}_m'' \sim \mathcal{D}_m^{n_m/2}} \left[\mathcal{L}_{\mathcal{D}_m}\left(h^{(1)}_{\mathcal{S}_m'', \mathcal{S}'}\right)\right] - 2\mathcal{L}_{\mathcal{D}_m}\left(h_m^*\right) \leq$$

$$\left\{\gamma_1 + \gamma_2 \cdot \left[\mathcal{L}_{\mathcal{D}_m}\left(h_{\mathcal{S}'}\right) - \mathcal{L}_{\mathcal{D}_m}\left(h_m^*\right)\right]\right\} \times \underbrace{\mathop{\mathbb{E}}_{\mathcal{S}_{m,\mathcal{X}}'' \sim \mathcal{D}_{m,\mathcal{X}}^{n_m/2},\, \mathbf{x} \sim \mathcal{D}_{m,\mathcal{X}}} \left[d\left(\phi_{h_{\mathcal{S}'}}(\mathbf{x}), \phi_{h_{\mathcal{S}'}}\left(\pi^{(1)}_{\mathcal{S}_m''}(\mathbf{x})\right)\right)\right]}_{\triangleq \mathcal{T}_{\mathcal{S}'}}, \tag{34}$$

where $\mathcal{S}_{m,\mathcal{X}}''$ denotes the set of input features in the dataset $\mathcal{S}_m''$ and $\mathcal{D}_{m,\mathcal{X}}$ the marginal distribution of $\mathcal{D}_m$ over $\mathcal{X}$. Note that $\mathcal{S}_m''$ is independent from $\mathcal{S}'$.

As in the proof of (Shalev-Shwartz and Ben-David, 2014, Theorem 19.3), let T be an integer to be precised later on. We consider $r = T^p$ and $C_1, \ldots, C_r$ to be the cover of the set $[0,1]^p$ using boxes with side $1/T$. We bound the term $\mathcal{T}_{\mathcal{S}'}$ independently from $\mathcal{S}'$ as follows

$$\mathop{\mathbb{E}}_{\mathcal{S}_m'' \sim \mathcal{D}_{m,\mathcal{X}}^{n_m/2},\, \mathbf{x} \sim \mathcal{D}_{m,\mathcal{X}}} \left[d\left(\phi_{h_{\mathcal{S}'}}(\mathbf{x}), \phi_{h_{\mathcal{S}'}}\left(\pi^{(1)}_{\mathcal{S}_m''}(\mathbf{x})\right)\right)\right] \leq \sqrt{p}\left(\frac{2T^p}{n_m e} + \frac{1}{T}\right). \tag{35}$$

If we set $\epsilon = 2\left(\frac{2}{n_m}\right)^{\frac{1}{p+1}}$ and $T = \lceil 1/\epsilon \rceil$, it follows $1/\epsilon \leq T < 2/\epsilon$ and then

$$\mathop{\mathbb{E}}_{\mathcal{S}_m'' \sim \mathcal{D}_{m,\mathcal{X}}^{n_m/2},\, \mathbf{x} \sim \mathcal{D}_{m,\mathcal{X}}} \left[d\left(\phi_{h_{\mathcal{S}'}}(\mathbf{x}), \phi_{h_{\mathcal{S}'}}\left(\pi^{(1)}_{\mathcal{S}_m''}(\mathbf{x})\right)\right)\right] \leq \sqrt{p}\left(\frac{2(2/\epsilon)^p}{n_m e} + \epsilon\right) \tag{36}$$

$$= \sqrt{p}\left(\frac{1}{e} + 2\right)\left(\frac{2}{n_m}\right)^{\frac{1}{p+1}} \tag{37}$$

$$\leq 6\frac{\sqrt{p}}{\sqrt[p+1]{n_m}}. \tag{38}$$

Thus,

$$\mathop{\mathbb{E}}_{\mathcal{S}_m' \sim \mathcal{D}_m^{n_m}} \left[\mathcal{L}_{\mathcal{D}_m}\left(h^{(1)}_{\mathcal{S}_m'', \mathcal{S}'}\right)\right] \leq 2\mathcal{L}_{\mathcal{D}_m}\left(h_m^*\right) + 6\frac{\sqrt{p}}{\sqrt[p+1]{n_m}}\left\{\gamma_1 + \gamma_2 \cdot \left[\mathcal{L}_{\mathcal{D}_m}\left(h_{\mathcal{S}}\right) - \mathcal{L}_{\mathcal{D}_m}\left(h_m^*\right)\right]\right\}. \tag{39}$$

□

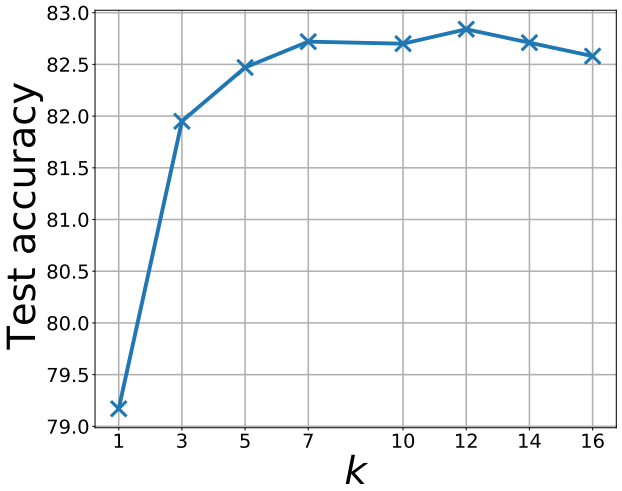

(a) CIFAR-10.

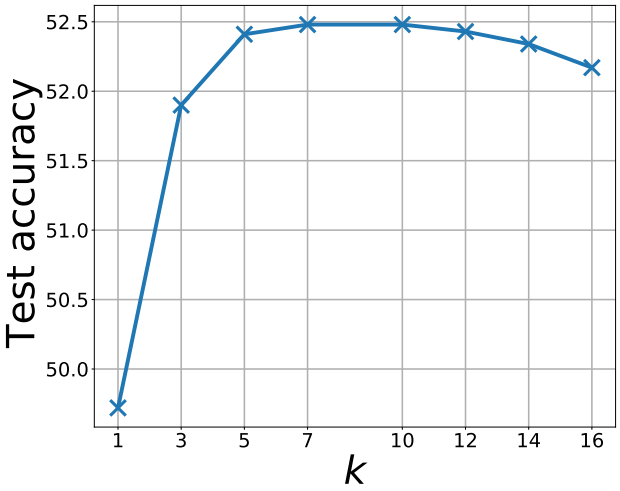

(b) CIFAR-100.

Figure 5. Test accuracy vs number of neighbors k.

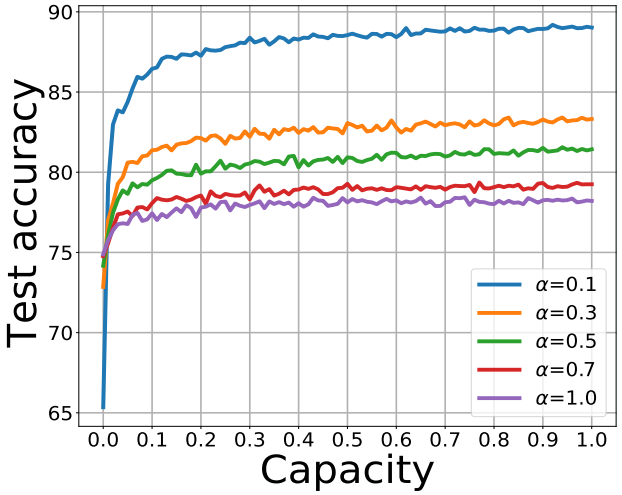

(a) CIFAR-10.

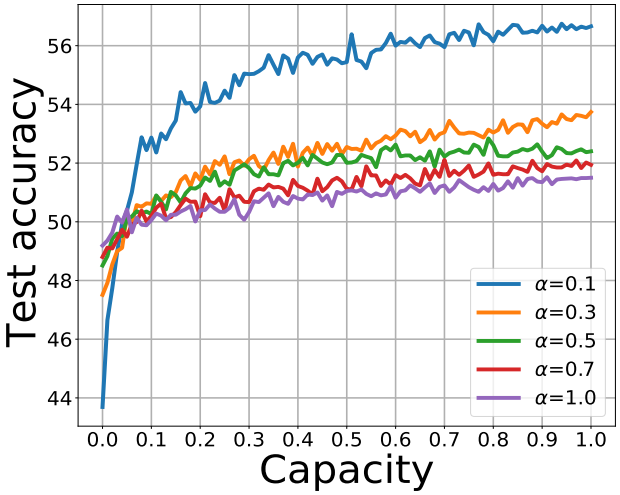

(b) CIFAR-100.

Figure 6. Test accuracy vs capacity (local datastore size) when the global model is retrained for each value of α. The capacity is normalized with respect to the initial size of the client's dataset partition. Smaller values of α correspond to more heterogeneous data distributions across clients. The curves start from different accuracy values for zero capacity, but are qualitatively similar to those in Figure 1 for large capacities. As expected, the global model performs worse the more heterogeneous the local distributions are, but the local model is able to compensate such effect (at least partially) as far as the datastore is large enough.

B. Additional Experiments

Effect of kernel scale parameter σ. We consider distance metrics of the form

$$\forall \mathbf{z}, \mathbf{z}' \in \mathbb{R}^p;\ d_\sigma\left(\mathbf{z}, \mathbf{z}'\right) = \frac{\|\mathbf{z} - \mathbf{z}'\|_2}{\sigma}, \tag{40}$$

where $\sigma \in \mathbb{R}^+$ is a scale parameter. Figure 7 shows that `kNN-Per`'s performance is not highly sensitive to the selection of the length scale parameter, as scaling the Euclidean distance by a constant factor σ has almost no effect for values of σ between 0.1 and 1000.

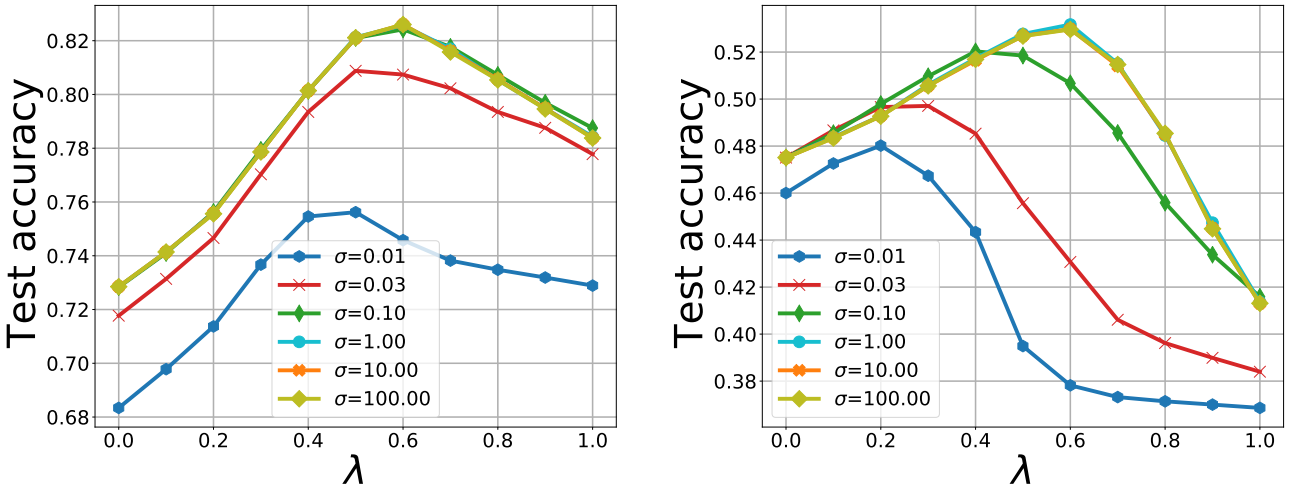

(a) CIFAR-10.

(b) CIFAR-100.

Figure 7. Test accuracy vs the interpolation parameter λ for different values of the kernel scale parameter σ.

Effect of datastore's size on the optimal λ. Figure 8 shows the effect of the local number of samples n_m on the optimal mixing parameter λ_{opt} (evaluated on the client's test dataset). The number of samples changes across clients and, for the same client, with different values of the capacity. The figure shows a positive correlation between the local number of samples and the optimal mixing parameter and then validates the intuition that clients with more samples tend to rely more on the memorization mechanism than on the base model, as captured by the generalization bound from Theorem 4.1.

Effect of hardware heterogeneity. In our experiments above, clients' local datasets had different size, which can also be due to different memory capabilities. In order to investigate more in depth the effect of system heterogeneity, we split the new clients in two groups: "weak" clients with normalized capacity $1/2 - \Delta C$ and "strong" clients with normalized capacity $1/2 + \Delta C$, where $\Delta C \in (0, 1/2)$ is a parameter controlling the hardware heterogeneity of the system. Note that the total amount of memory in the system is constant, but varying ΔC changes its distribution across clients from a homogeneous scenario ($\Delta C = 0$) to an extremely heterogeneous one ($\Delta C = 0.5$). Figure 9 shows the effect of the hardware heterogeneity, as captured by ΔC. As the marginal improvement from additional memory is decreasing (see, e.g., Fig. 1) the gain for strong clients does not compensate the loss for weak ones. The overall effect is then that the average test accuracy decreases as system heterogeneity increases.

Adding compression techniques. `kNN-Per` can be combined with nearest neighbours compression techniques as `ProtoNN` (Gupta et al., 2017). `ProtoNN` reduces the amount of memory required by jointly learning 1) a small number of prototypes to represent the entire training set and 2) a data projection into a low dimensional space. We combined `kNN-Per` and `ProtoNN` and explored both the effect of the number of prototypes and the projection dimension used in `ProtoNN`. For each client, the number of prototypes is set to a given fraction of the total number of available samples. We refer to this quantity also as capacity. We varied the capacity in the grid $\{i \times 10^{-1}, i \in [10]\}$, and the projection dimension in the grid $\{i \times 100, i \in [12]\} \cup \{1280\}$. Note that smaller projection dimension and less prototypes correspond to a smaller memory footprint, suited for more restricted hardware. Our implementation is based on `ProtoNN`'s official.[5] Figure 11a shows that, on CIFAR-10, `ProtoNN` allows to reduce the `kNN-Per`'s memory footprint by a factor four (using $n_m/3$ prototypes and projection dimension 1000) at the cost of a limited reduction in test accuracy (82.3% versus 83.0% in Table 2). Note that `kNN-Per` with `ProtoNN` still outperforms all other methods. On CIFAR-100, `ProtoNN`'s compression techniques appear less advantageous: the approach loses about 3 percentage points (52.1% versus 55.0% in Table 2) while only reducing memory requirement by 20%.

Effect of global model's quality. Assumption 4 stipulates that the smaller the expected loss of the global model, the more accurate the corresponding representation. As representation quality improves, we can expect that kNN accuracy

[5] https://github.com/Microsoft/EdgeML.

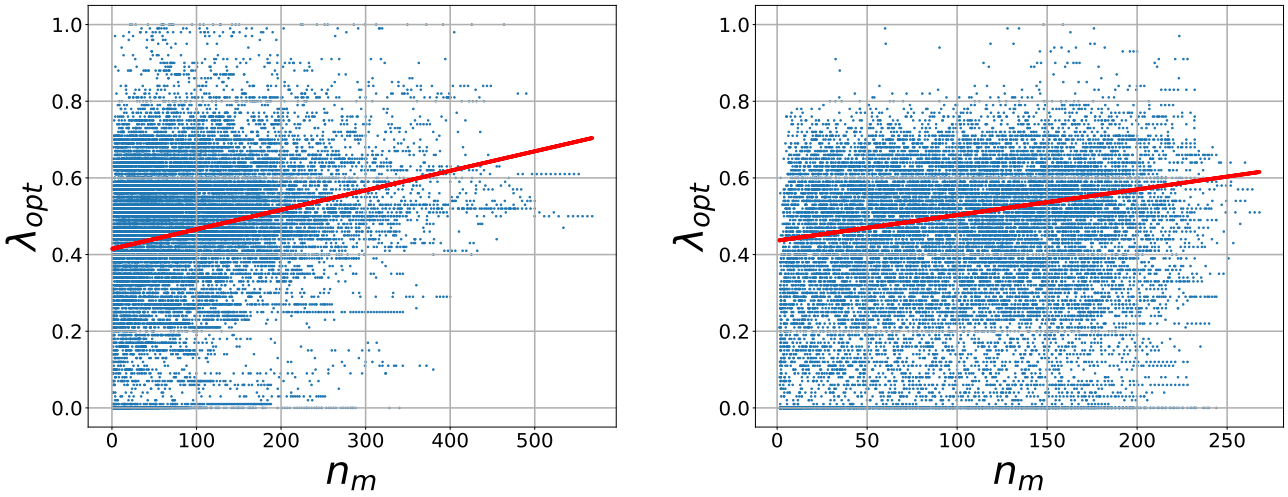

(a) CIFAR-10.

(b) CIFAR-100.

Figure 8. λ_{opt} vs local number of samples n_m.

improves too. This effect is quantified by Lemma A.2, where the loss of the local memorization mechanism is upper bounded by a term that depends linearly on the loss of the global model. In order to validate this assumption, we study the relation between the test accuracies of the global model and `kNN-Per`. In particular, we train two global models, one for CIFAR-10 and the other for CIFAR-100, in a centralized way, and we save the weights at different stages of the training, leading to global models with different qualities. Figure 12 shows the test accuracy of `kNN-Per` with $\lambda = 1$ (i.e., when only the knn predictor is used) as a function of the global model's test accuracy for different levels of heterogeneity on CIFAR-10 and CIFAR-100 datasets. We observe that, quite unexpectedly, the relation between the two accuracies is almost linear. The experiments also confirm what observed in Fig. 1: `kNN-Per`performs better when local distributions are more heterogeneous (smaller α). Similar plots with λ optimized locally at every client are shown in Fig. 13.

Robustness to distribution shift. As previously mentioned, `kNN-Per` offers a simple and effective way to address statistical heterogeneity in a dynamic environment where client's data distributions change after training. We simulate such a dynamic environment as follows. Client m initially has a datastore built using instances sampled from a data distribution $\mathcal{D}_m$. For time step $t < t_0$, client m receives a batch of $n_m^{(t)}$ instances drawn from $\mathcal{D}_m$. At time step t_0, we suppose that a data distribution shift takes place, i.e., for $t_0 \leq t \leq T$, client m receives $n_m^{(t)}$ instances drawn from a data distribution $\mathcal{D}'_m \neq \mathcal{D}_m$. Upon receiving new instances, client m may use those instances to update its datastore. We consider 3 different strategies: (1) *first-in-first-out* (FIFO) where, at time step t, the $n_m^{(t)}$ oldest samples are replaced by the newly obtained samples; (2) *concatenate*, where the new samples are simply added to the datastore; (3) *fixed datastore*, where the datastore is not updated at all. In our simulations, we consider CIFAR-10/100 datasets with $M = 100$ clients. Once again, we used a symmetric Dirichlet distribution to generate two datasets for every client. In particular, for each label y we sampled two vectors p_y and p'_y from a Dirichlet distribution of order $M = 100$ and parameter $\alpha = 0.3$. Then, for client m, we generated two datasets $\mathcal{S}_m$ and $\mathcal{S}'_m$ by allocating $p_{y,m}$ and $p'_{y,m}$ fraction of all training instances of class y.[6] Both $\mathcal{S}_m$ and $\mathcal{S}'_m$ are partitioned into training and test sets following the original CIFAR training/test data split. Half of the training set obtained from $\mathcal{S}_m$ is stored in the datastore, while the rest is further partitioned into t_0 batches $\mathcal{S}_m^{(0)}, \ldots, \mathcal{S}_m^{(t_0-1)}$. These batches are the new samples arriving at client m. Similarly, $\mathcal{S}'_m$ is partitioned into $T - t_0$ equally sized batches. Figure 14 shows the evaluation of the test accuracy across time. If clients do not update their datastores, there is a significant drop in accuracy as soon as the distribution changes at $t_0 = 50$. If datastore are updated using FIFO, we observe some random fluctuations for the accuracy for $t < t_0$, as repository changes affect the kNN predictions. While accuracy inevitably drops for $t = t_0$, it then increases as datastores are progressively populated by instances from the new distributions. Once all samples from the previous distributions are evicted, the accuracy settles around a new value (higher or lower than the one for $t < t_0$ depending on the difference between the new and the old distributions). If clients keep adding new samples to their datastores (the

[6] We always make sure that $|\mathcal{S}_m| \leq |\mathcal{S}'_m|$.

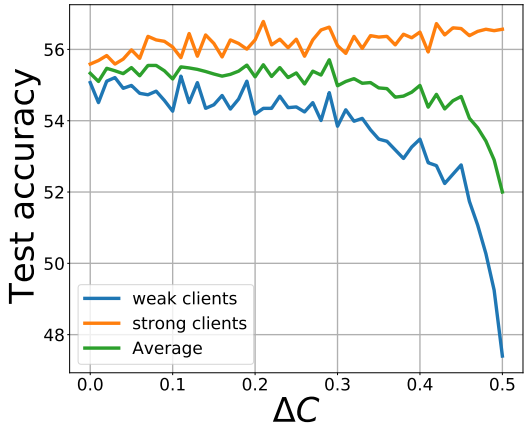

Figure 9. Effect of system heterogeneity across clients on CIFAR-100 dataset. The size of the local datastore increases (resp. decreases) with ΔC for strong (resp. weak) clients.

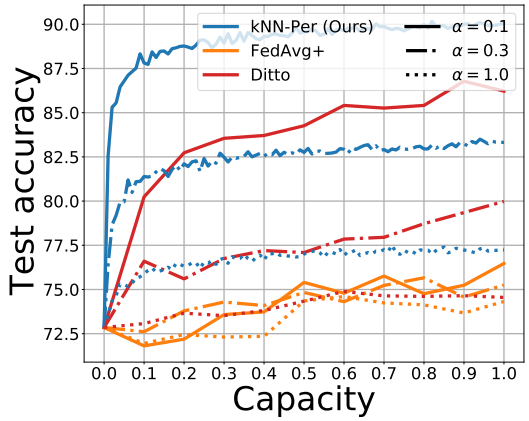

Figure 10. Test accuracy vs capacity (local datastore size) for different methods on CIFAR-10. The capacity is normalized with respect to the initial size of the client's dataset partition.

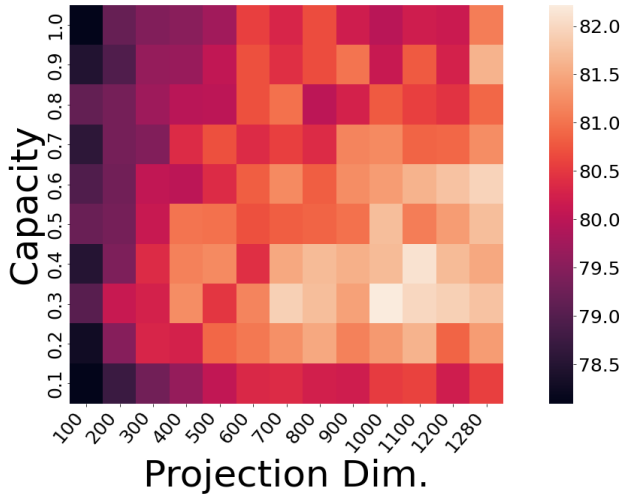

(a) CIFAR-10.

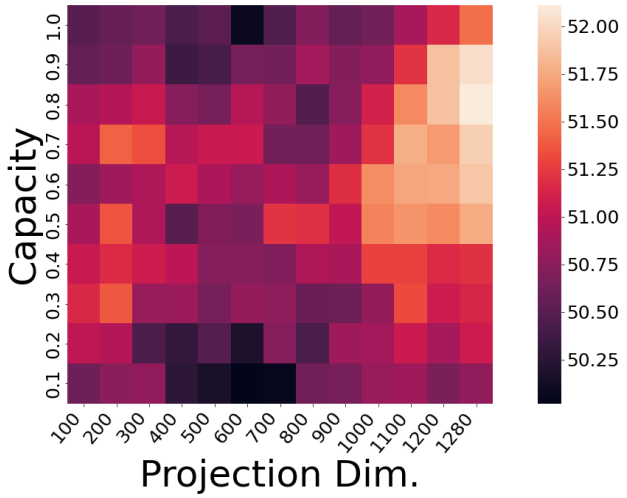

(b) CIFAR-100.

Figure 11. Test accuracy when the kNN mechanism is implemented through `ProtoNN` for different values of projection dimension and number of prototypes (expressed as a fraction of the local dataset). CIFAR-10 (left) and CIFAR-100 (right) datasets.

"concatenate" strategy), results are similar, but 1) accuracy increases for $t < t_0$ as the quality of kNN predictors improves for larger datastores, 2) accuracy increases also for $t > t_0$, but at a slower pace than what observed under FIFO, as samples from the old distribution are never evicted.

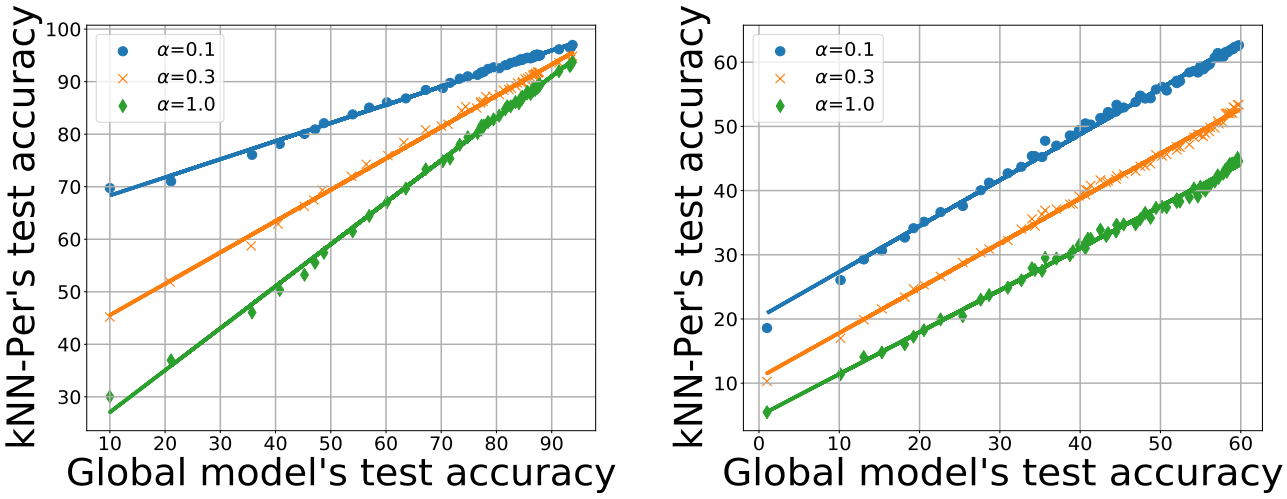

(a) CIFAR-10. (b) CIFAR-100.

Figure 12. Effect of the global model quality on the test accuracy of `kNN-Per` with $\lambda_m = 1$ for each $m \in [M]$.

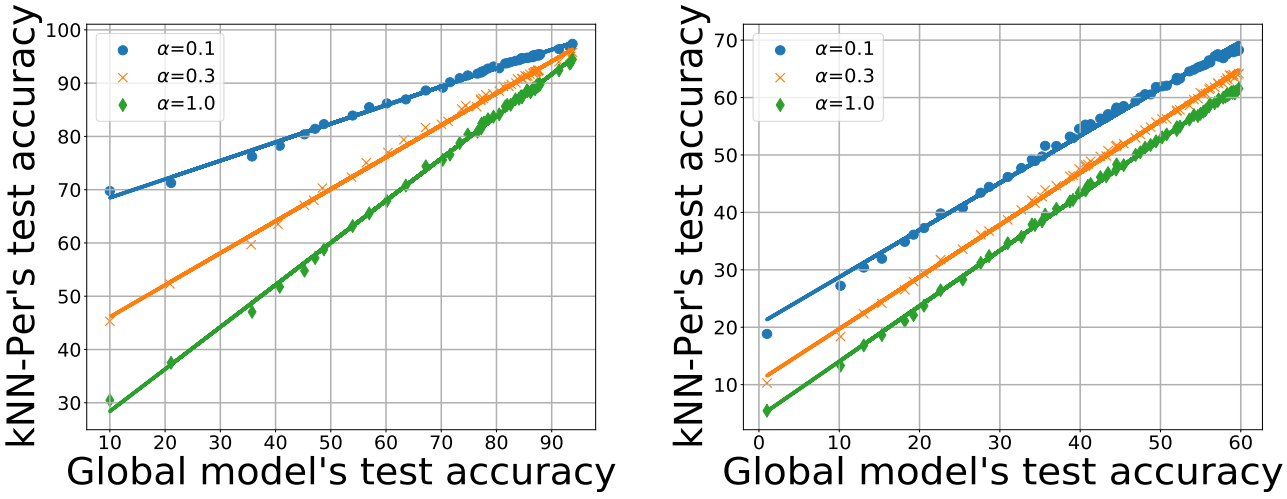

(a) CIFAR-10. (b) CIFAR-100.

Figure 13. Effect of the global model quality on the test accuracy of `kNN-Per` with λ_m tuned per client.

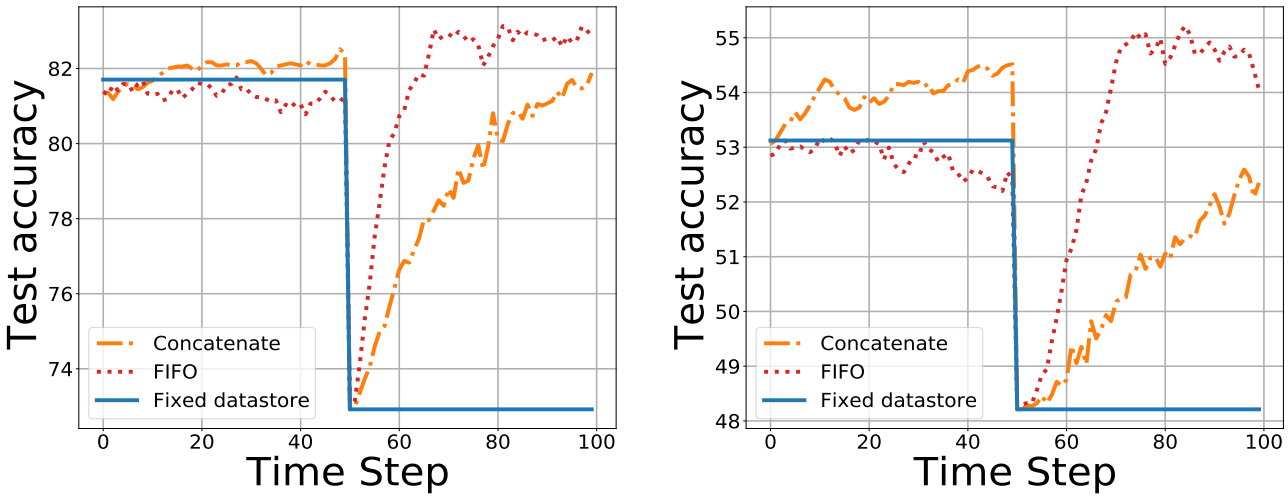

(a) CIFAR-10.

(b) CIFAR-100.

Figure 14. Test accuracy when a distribution shift happens at time step $t_0 = 50$ for different datastore management strategies.